Renewable Energy 257 (2026) 124732

Contents lists available at ScienceDirect

Renewable Energy

journal homepage: www.elsevier.com/locate/renene

Performance loss rate and benchmarking of c-Si and thin-film PV modules considering thermal and spectral effects at a low-latitude site

Miguel Ángel Sevillano-Bendezú [a,b,*], Luis Ángel Conde [a], Michael Anthony García [a], José Rubén Angulo [a], Juan de la Casa [c], José María Ripalda [b], Jan Amaru Töfflinger [a,**]

[a] Departamento Académico de Ciencias, Sección Física, Pontificia Universidad Católica del Perú, Av. Universitaria 1801, 15088, Lima, Peru
[b] Instituto de Micro y Nanotecnología (IMN-CNM), CSIC, Isaac Newton 8, Tres Cantos, 28760, Madrid, Spain
[c] Center for Advanced Studies in Earth Sciences, Energy and Environment (CEACTEMA). University of Jaén, Campus Las Lagunillas, 23071, Jaén, Spain

ARTICLE INFO

Keywords:
PV module degradation
Outdoor I-V curve monitoring
PV performance assessment
Performance Loss Rate
Ensemble PLR analysis

ABSTRACT

Field-based assessment of photovoltaic (PV) module performance provides key insights for accurate lifespan prediction and reliability analysis. However, two significant research gaps remain: the scarcity of long-term evaluations in low-latitude regions and the limited application of established ensemble methods under diverse climatic conditions. This study presents a long-term field performance analysis of eight PV technologies installed in Lima, Peru, a subtropical desert climate at low latitude. Module Performance Ratio (MPR) was evaluated considering the effects of measured temperature and spectral variations. For c-Si-based modules, thermal losses ranged from −2.7 % to −4.3 %, while thin-film modules exhibited smaller thermal impacts (−2.2 % to −2.6 %). Spectral losses in c-Si modules ranged from −0.7 % to −1.5 %. Conversely, a-Si modules recorded spectral gains of 5.7 %. Additional analysis of open-circuit voltage, short-circuit current, and fill factor revealed distinct performance degradation pathways across technologies. Ensemble-derived Performance Loss Rates (PLR), combined with climate-influencing factors, enabled benchmarking and 25-year energy yield projections. Our reported PLRs of up to −1.61 %/year for c-Si slightly exceed reported global-median PLRs, suggesting detrimental effects of Lima's high humidity and UV exposure. Projections indicate that in Lima HIT modules may outperform IBC and PERT technologies, underscoring the value of region-specific, long-term PV performance studies.

1. Introduction

Global solar photovoltaic (PV) capacity experienced an exceptional year-on-year growth rate reaching additional 602 GW in 2024, surpassing the global cumulative 2.2 TW by the year's end. This remarkable expansion accounted for ~81 % of all new renewable energy capacity added worldwide, exceeding any expectations of solar analysts. Anticipated annual growth of ~3.4 TW should further surpass the yearly last mark on the way to reaching the target of global 75 TW by 2050 as part of the energy transition deployment goals [1]. This continuous expansion of solar PV technology worldwide implies that new module designs with changing Bill of Materials (BoM) are being developed and deployed in huge quantities faster than we can detect failure mechanisms and understand degradation modes [2]. Building reliability and ensuring the service life in the PV technology instills confidence among potential end users and financiers, enabling faster and more widespread deployment in a synergistic feedback loop. However, this increasing deployment makes accurately predicting the service life of incoming modules more challenging. Field performance assessment provides essential data for implementing appropriate accelerated testing and standards. This helps close the PV reliability learning cycle, improving the long-term service life prediction [3]. In the current Terawatt era, conducting detailed, long-term performance assessments at the module level has become more valuable than ever. Insights gained from existing technologies are instrumental in establishing best practices and standards for future modules, thereby mitigating the risks associated with the large-scale deployment of innovative products. Besides PV module failure modes and mechanisms, specific-climate impacts on durability have not been comprehensively elucidated [4]. Despite knowing that factors such as temperature, solar spectrum variation, and low irradiance influence

* Corresponding author. Instituto de Micro y Nanotecnología (IMN-CNM), CSIC, Isaac Newton 8, Tres Cantos, 28760, Madrid, Spain.
** Corresponding author. Departamento Académico de Ciencias, Sección Física, Pontificia Universidad Católica del Perú, Av. Universitaria 1801, 15088, Lima, Peru.
E-mail addresses: m.sevillano@csic.es (M.Á. Sevillano-Bendezú), japalominot@pucp.edu.pe (J.A. Töfflinger).

https://doi.org/10.1016/j.renene.2025.124732
Received 16 August 2025; Received in revised form 6 November 2025; Accepted 7 November 2025
Available online 10 November 2025

energy yield performance, their effects on long-term performance remain unclear, making specific climate studies worthwhile [5]. There are substantial gaps in the literature concerning technologies and geographical regions regarding field performance at both module and system levels [6]. Most comparative long-term studies predominantly report on sites located at mid-latitudes, often featuring continental or temperate climates [7], as exemplified by research in Eastern Europe [8]. Similarly, many reliability assessments analyze performance and degradation in the well-represented mid-latitude temperate zones [9]. Nonetheless, there is still a noticeable geographical gap due to the scarcity of research in dissimilar locations, e.g., at low latitudes and in the Southern Hemisphere [10].

The Performance Loss Rate (PLR) is a standard metric used to evaluate the performance of PV systems and modules. It measures the change in the annualized Performance Ratio relative to the first year, capturing both reversible (e.g., soiling and shading) and irreversible effects (e.g., module degradation) [11]. Focusing on the module level helps mitigate uncertainties in the calculation caused by Balance of System (BoS) degradation and wiring/connection losses at the system level. However, the computation of PLR involves significant complexity due to the myriad of approaches and pipelines in the PLR metric. This complexity exists despite using a common framework comprising five key steps: (1) exploratory data analysis for assessing data quality and grading, (2) cleaning and filtering of input data, (3) selection of performance metrics, corrections, and aggregating data, and (4) correcting time series features and (5) statistical modeling of PLR [12]. Typically, applying each step is up to the discretion of the analyst performing the calculation, contributing to a lack of uniformity in the reliable computation of PLR [12]. PLR is commonly assumed to be linear, and linear PLR statistical methods are typically categorized into regression methods, including Ordinary Least Squares (OLS) regression [13], Classical Seasonal Decomposition (CSD) [12], and methods based on a loss rate distribution, such as the Year-on-Year (YoY) method [14]. However, in many cases, the linear behavior of PLR is not realistic due to incorporated reversible and irreversible effects that can occur at different stages of the PV module lifetime, such as potential-induced degradation (PID) or early life failure modes. Recent studies have introduced methodologies to capture non-linear trends of PLR [15]. Non-linear PLR assessment on the system level represents a potential key performance indicator in the O&M strategy, e.g., in detecting performance anomalies [13]. However, assuming linear PLR remains the most standardized and straightforward comparable approach to handle and report within the current context of long-term PV module performance assessment [15]. The `RdTools` open-source library, developed in Python, implements the above PLR linear statistical models and a comprehensive set of tools for conducting technical analysis of PV time series data [16]. The ensemble approach is considered the most reliable procedure for calculating PLR, as it involves comparing various statistical methods using diverse performance metrics and filtering approaches and subsequently deriving the PLR as the mean inlier [15]. This approach is best used for high-resolution/high-quality data [17]. Further investigation into the reliability of the ensemble approach is necessary to gain insights into its performance under various stress conditions, such as varying climate, variable number of pipelines, and different PV technologies [4].

Hence, based on the information provided above, we identify two key gaps in PV lifespan and reliability assessment.

1. There is a scarcity of literature addressing long-term performance assessment in low-latitude areas and the Southern Hemisphere, particularly on the module level.
2. The applicability of the recent ensemble approach across varying climate conditions and PV technologies.

The present work aims to address these two gaps by: (1) Assessing the long-term performance on the module level based on measured I-V curves in Lima, Peru, a region characterized by a desert and humid climate near the equator. This assessment encompasses eight distinct PV module technologies monitored for over five years: Al-BSF, HIT, PERT, IBC, PERC, a-Si/μc-Si, a-Si, and CIGS. We report the most influential figures of merit in PV performance, such as the Module Performance Ratio (MPR) and climate-specific loss factors attributed to thermal influences and sun spectrum variations. Furthermore, we analyze the losses of the main performance parameters (V_{oc}, I_{sc}, FF). (2) We implement the ensemble approach to compute the mean PLR, following a rigorous data workflow and addressing three different performance metrics: the MPR, the Module Performance Index (MPI), and the operational nominal power (P_{nom}). The PLR computation considered three linear statistical methods, OLS, YoY, and CSD, covering nine pipelines in total. Finally, we benchmark the eight technologies in terms of performance, representing the first study of this kind conducted in the region and contributing to the existing research gaps in PV module durability and reliability.

2. Experimental and methodology

2.1. The Outdoor Photovoltaic Research Laboratory in Lima, Peru

The present study gathered experimental data from the Outdoor Photovoltaic Research Laboratory at the Pontificia Universidad Católica del Perú (PUCP) in the coastal area of Lima (latitude 12°4′S, longitude 77°4′W), in Peru (see Fig. 1). According to the Köppen-Geiger Climate Classification, Lima is officially classified as having a hot desert climate (Bwh) [18]. However, Lima's average temperature is lower than that of a typical Bwh area [19], and its high annual relative humidity levels make Lima humid and subtropical, with mostly cloudy days in winter [20], giving the city a uniquely distinctive climate for the region. Lima's climate peculiarities make it attractive to evaluate the long-term performance of PV modules. The laboratory is well-equipped with meteorological sensors to monitor broadband and spectral irradiance, ambient temperature, wind speed, and moisture, as well as monitor the performance of different PV module technologies, as depicted in Fig. 1 (a).

Fig. 1 (b) illustrates the schematic of the monitoring setup. The multiplexer system allows for the individual tracing of the I-V curve alongside the synchronized meteorological measurements. The setup executes this process sequentially for each module.

The modules are tilted at 20° facing north. The I-V tracer is based on a capacitive load, as detailed in Montes-Romero et al. (2017) [21] and employed in Sevillano-Bendezú et al. (2024) [20]. The I-V tracer exhibited very low uncertainties of around 0.58 % for the short-circuit current (I_{sc}) and 0.23 % for the open-circuit voltage (V_{oc}) in Ref. [22]. The setup uses two digital multimeters, Keysight 34465A, to measure the I-V curve of each module, with recording times ranging from 2 to 40 s depending on the current and irradiance. We measured the broadband irradiances, including Global Horizontal Irradiance (GHI) and plane-of-array irradiance (G_{poa}), with two EKO MS-80 pyranometers, while an EKO MS711 spectroradiometer captures the spectral irradiance in the plane-of-array. We placed the spectroradiometer horizontally from 2023 on. Using spectral data, we calculated the Average Photon Energy (APE) within the range of 350–1050 nm, as detailed in Ref. [23]. This index indicates whether the solar spectrum is bluer or redder than the AM1.5G spectrum, depending on whether it is higher or lower than 1.876 eV (the APE for the AM1.5G spectrum [24,25]), respectively.

We defined the module temperature as the average of the temperatures measured using two class B sensors at the PV modules' rear side center and corner. We synchronously measured the I-V curves for each PV module every 5 min with all meteorological parameters. Additionally, we cleaned the modules ~ biweekly to minimize soiling losses. For more details on the PV module characterization system and its components, see Conde et al. (2019) [26].

Table 1 summarizes the equipment used for data collection, including the brand and model.

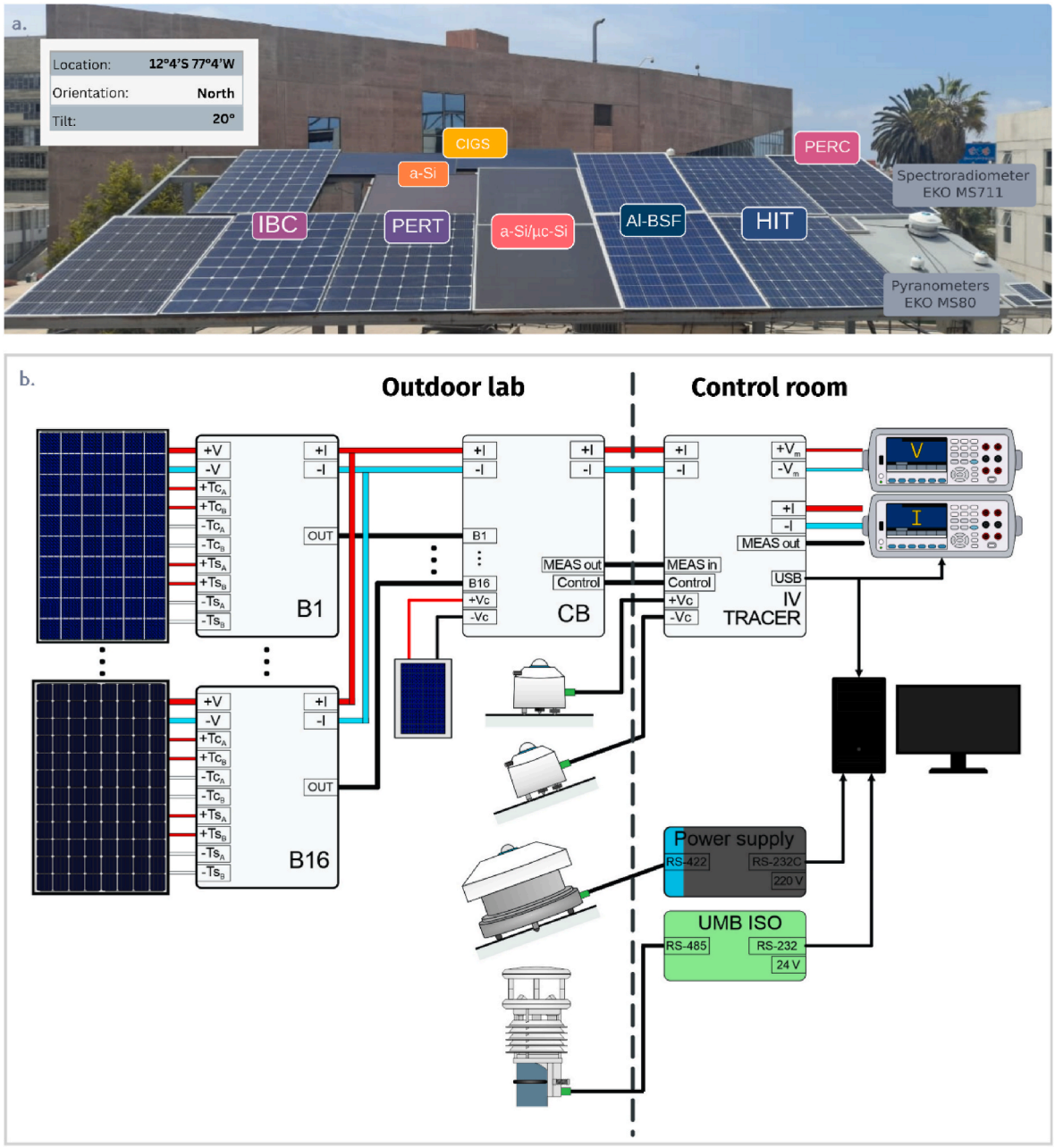

Fig. 1. Outdoor Photovoltaic Research Laboratory in Lima, Peru: (a) Photograph of the studied c-Si and thin-film PV module technologies and the meteorological sensors employed. (b) Schematic view of the laboratory setup, including PV modules, control box (CB), I–V tracer with digital multimeters, pyranometers, spectroradiometer, weather station, and monitoring PC.

This study selected eight PV modules using different technologies. Based on crystalline Si (c-Si) wafer: p-type multi-crystalline Si (mc-Si) Aluminium Back Surface Field (Al-BSF), n-type monocrystalline Si (mono-Si) Heterojunction with Intrinsic Thin layer (HIT), n-type mono-Si Passivated Emitter Rear Totally diffused (PERT), n-type mono-Si Interdigitated Back Contact (IBC), p-type mono-Si Passivated Emitter and Rear Contact (PERC), and based on a thin-film absorber material: Amorphous silicon/microcrystalline silicon (a-Si/µc-Si) tandem, amorphous silicon (a-Si), and Copper Indium Gallium Selenide (CIGS).

Table 2 presents an overview of the electrical characteristics of the PV modules under Standard Test Conditions (STC), including the maximum power, efficiency, I_{sc}, V_{oc}, the current (I_{mp}) and voltage (V_{mp}) at maximum power, the temperature coefficients for power (γ), current (α) and voltage (β), and nominal operating cell temperature (NOCT). We derived these parameters and inferred the approximate year of release from the datasheets.

Fig. 2 illustrates the annual percentage of power delivered by the HIT module in 2022 as a function of irradiance and module temperature. Based on the available data, achieving STC conditions in Lima is unlikely, as there are no data points corresponding to 1000 W/m^2 and 25 °C. Consequently, the nominal parameters appear unrealistic for forecasting the energy yield under field conditions. Furthermore, two notable regions exhibit the highest productivity: the first occurs under low-irradiance conditions between approximately 200 and 400 W/m^2, primarily associated with the frequent cloudy skies in winter; the second appears around 1000 W/m^2, corresponding to the frequent clear skies mainly in summer, as reported in [20].

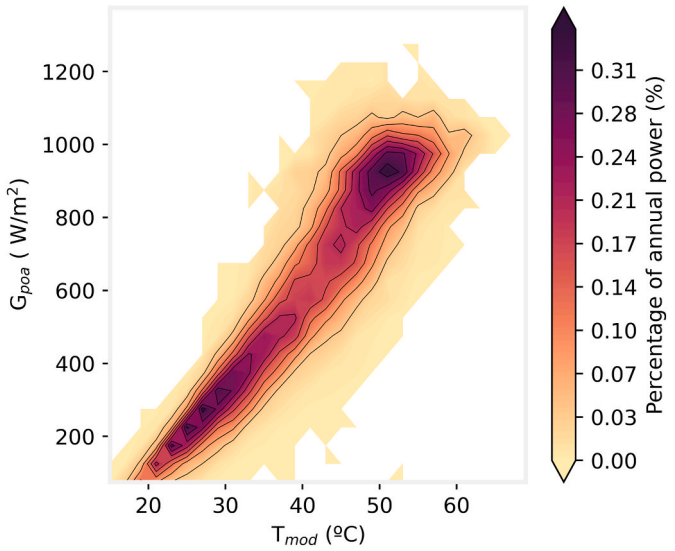

Fig. 2. Percentage of annual power for the HIT module in 2022 as a function of the plane of array irradiance and the module temperature.

Table 1
Measurements setup description.

Measurement	Measuring instrument	Brand/Model
I-V curve	Capacitive load I-V tracer	[20–22]
T_{mod}	Pt100 Class B	RS/RTF-100-S4B-2.0-C8
T_{amb}	Weather Station	Lufft/WS 500
G_{POA}	Pyranometer	EKO/MS80
GHI	Pyranometer	EKO/MS80
Spectra	Spectroradiometer	EKO/MS711

2.2. PV technology-related spectral information

We retrieved spectral response data for the eight PV technologies from previous studies. These include Al-BSF, PERC, and PERT from Bryan et al. (2022) [29], a-Si/μc-Si from Ye et al. (2014) [27], HIT and IBC from Chantana et al. (2017) [28], and CIGS and a-Si from Sevillano-Bendezú et al. (2023) [24]. Subsequently, we calculated the relative External Quantum Efficiency (EQE) spectra, as outlined in Sevillano--Bendezú et al. (2023) [24]. EQE spectra are commonly used to represent the spectral behavior of a PV generator. Fig. 3 illustrates these relative EQEs with their corresponding calculated bandgaps.

2.3. Climatic effects corrections and performance metrics

This work calculates and corrects performance metrics, assuming the rated values (nameplate) in Table 2 as reference and initial state parameters. We conducted temperature corrections following the IEC 61724–1:2021 [30], utilizing T_{mod} and STC-γ as primary inputs. We relied on the Spectral Mismatch Factor (SMM) from IEC 60904–7:2019 [31] to perform the spectral corrections for the single junction technologies, utilizing the spectral responses (relative EQEs) from Fig. 3 and measured spectra as inputs. In the case of the a-Si/μc-Si tandem module, the spectral correction accounted for the current-matching effect by selecting the SMM of the current-limiting subcell, as adapted from Rodrigo et al. (2017) [32]. The spectral correction covered the 300–4000 nm range by extrapolating the measured spectra [23].

This study covered the most common performance metrics on the module level, incorporating each climatic correction described above as follows.

2.3.1. Module Performance Ratio

The MPR definition is equivalent to that of the PV system performance ratio [33].

$$MPR = \frac{Y_{mod}}{Y_{ref}} = \frac{E_{mod}/P_{STC}}{H_{POA}/G_{STC}} \quad (1)$$

The module Energy Yield (Y_{mod}) and the Reference Yield (Y_{ref}) represent the ratios of integrated energy (E_{mod}) and irradiation (H_{POA}) to power and irradiance under STC (P_{STC} and G_{STC}).

MPR is intrinsically linked to local climatic conditions. In this paper, we quantify the impact of T_{mod} variations ($\Delta MPR_{Temperature}$) on PV performance by calculating the difference between the temperature-corrected MPR ($MPR_{T\to 25^\circ C}$).) and the uncorrected MPR. Conversely, the effects attributed to shifts in spectral distribution ($\Delta MPR_{spectrum}$) are evaluated by examining the difference between the spectrum- and temperature-corrected MPR ($MPR^{G_i\to AM1.5G}_{T\to 25^\circ C}$) and the $MPR_{T\to 25^\circ C}$. Both metrics are expressed as percentage changes, indicating performance

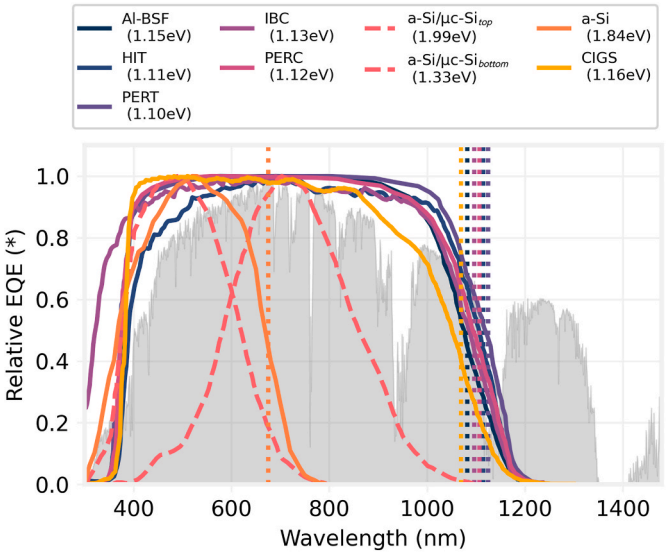

Fig. 3. Relative EQEs of the 8 different PV technologies and the AM1.5G photon flux in the background [24,27–29]. The corresponding calculated bandgap energy of the absorber material is indicated in brackets and marked by vertical dotted lines.

Table 2
Main rated parameters of the 8 PV modules from the manufacturer datasheets.

Tech	Approx. Year of release	Max. Power (W)	Efficiency (%)	I_{sc} (A)	V_{oc} (V)	I_{mp} (A)	V_{mp} (V)	γ (%/C°)	α (%/C°)	β (%/C°)	NOCT (°C)
Al-BSF	2016	270	16.5	9.32	37.9	8.75	30.8	−0.41	0.053	−0.32	45
HIT	2016	330	19.7	6.07	69.7	5.7	58.0	−0.26	0.055	−0.23	44
PERT	2019	345	20.1	10.57	41.2	9.89	34.9	−0.36	0.030	−0.27	42
IBC	2018	370	21.4	10.82	42.8	10.01	37.0	−0.30	0.040	−0.23	44
PERC	2019	315	19.3	9.92	40.73	9.49	33.2	−0.39	0.040	−0.27	43
a-Si/μc-Si	2011	128	9.0	3.45	59.8	2.82	45.4	−0.24	0.070	−0.30	44
a-Si	2008	60	6.31	1.19	91.8	0.9	67.0	−0.23	0.075	−0.31	44
CIGS	2017	115	14.3	2.07	77.2	1.94	59.3	−0.23	0.011	−0.30	46

gains or losses relative to zero.

2.3.2. Effective nominal power

The operational effective nominal power (P_{nom}) of a PV module reflects its power during operation, translated to STC. This metric is determined by correcting for temperature losses and considering high irradiances. P_{nom} encapsulates the impact of on-field phenomena such as module degradation and other losses like spectral mismatch and soiling, distinguishing it from P_{STC}. In this study, P_{nom} was calculated using the Kernel Density Estimation (KDE) approach as proposed by Angulo et al. (2024) [34].

2.3.3. Module Performance Index

Additionally, this study employed the Sandia Array Performance Model (SAPM) to electrically simulate each PV module, which computes the performance parameters, including V_{oc}, I_{sc}, maximum power point voltage (V_{mp}), and maximum power point current (I_{mp}). The main inputs comprise spectrally corrected G_{poa} and the measured T_{mod}. We calculated expected power by simply multiplying V_{mp} and I_{mp}. The `ModelChain` class in `pvlib` includes the SAPM model functionalities [35].

The MPI of the power output serves as a quantitative measure of the ratio between the actual delivered power of a PV module and its expected value [36]. Based on this definition, we similarly computed the MPI of V_{oc}, I_{sc}, and FF using the expected V_{mp}, I_{mp}, V_{oc}, I_{sc}.

2.3.4. Performance loss rate

The PLR metric quantitatively represents the variations in PV performance relative to an initial state, commonly reported in %/year. This study examines three PLR linear statistical models: OLS, YoY, and CSD. Each model includes a Monte Carlo-derived confidence interval (CI), as detailed in the `RdTools` documentation [16]. Our high-quality data supported using the 95 % CI, as recommended by the IEA PVPS report [12]. The ensemble approach combines different pipelines to create a single representative mean inlier PLR ($\overline{PLR}$) from these pipelines [15]. This study adapted the ensemble approach to encompass nine pipelines combining the MPR, P_{nom} and power MPI metrics alongside the OLS, YoY, and CSD statistical methods. We stuck to the five-step data workflow according to Lindig et al. (2022) [13], comprising: (a) Data quality analysis, (b) Cleaning and filtering, (c) Performance metric selection, (d) Feature corrections (e) Statistical model applications.

The following subsection outlines the general data processing procedures, including those followed by the PLR data workflow.

2.4. Data processing

Lindig et al. (2024) [37] emphasize the importance of data cleaning and filtering to derive reliable outcomes and valuable insights from KPI calculations. Our study initially excluded measurements from days characterized by scarce data availability of commonly peak illumination hours. We established criteria for a valid measurement day, requiring at least 80 % of measurements for Angle of Incidence (AoI) less than 40°. We reinforced this approach by implementing specific custom filters and constraints tailored to the measurement context (e.g., weather analysis, PV performance metrics calculation), which included the utilization of complete-year datasets to mitigate biases and uncertainties depending on the specific KPI. Thereby, we applied the following threshold to weather measurements when independently plotted.

- $5 < G_{poa} < 1500$ W/m^2
- $10 < T_{amb} < 35$ °C, adjusted to Lima's weather
- APE and SMM constrained to $AoI < 60°$ (to avoid the influence of large spectral variation in early mornings and late afternoons)

We implemented data-driven filters on the I-V curves utilizing the ubiquitous instantaneous nominal power (power $\times$ $G_{STC}/\ G_{poa}$) alongside key performance parameters, namely power, V_{oc}, and fill factor (FF). We ensure the distribution of these parameters is preserved within an integer distance of standard deviations from the mean in their respective units. We chose between 3 and 6 standard deviations depending on the PV technology, aiming to keep as many measurements as possible while removing outliers and malfunctions. Furthermore, a comprehensive visual inspection facilitated the exclusion of any remaining outliers within distributions that exhibited asymmetrical characteristics relative to the mean. Additionally, we systematically excluded IV curves corresponding to power outputs below 25 W/m^2. The parameters above were essential to assess performance metrics, besides supplementary measurements required for temperature, spectrum corrections, and aggregations. To this end, we confined G_{poa} to the previously indicated range and set T_{mod} between 13 and 70 °C, while we did not impose restrictions on the SMM when associated with performance metrics calculations.

We conducted aggregations over various time intervals, including days, weeks, months, and years, the last based on a complete operational cycle of 365 days. We differentiated the annual aggregation from the annual daily average, which is the simple average of daily aggregations, thereby yielding crucial statistical insights into a representative daily performance metric over a year. Additionally, we incorporated the complete datasets for the PLR calculation to capture most of the available intrinsic loss phenomena. Nonetheless, given the evident seasonal variations in the PR, we utilized only complete year datasets for this analysis. Finally, we truncated the measurement periods to facilitate a more equitable comparison in benchmarking the eight PV technologies. This meticulous collection of methodologies enabled a thorough analysis. In the results section, we specify the selected period for each analysis to clarify its intended purpose.

3. Results and analysis

3.1. Main meteorological parameters influencing the PV performance

The MPR indicates the performance of PV modules under real-world climatic conditions relative to their expected performance under STC. Consequently, this indicator represents an instrumental measure in elucidating how different climatic variables affect the performance of various PV modules [33]. The IEA-PVPS T13-20 report [38] provides a comprehensive overview of the principal factors affecting the MPR, including the significance of module temperature and variations in spectral distribution as key influencers. We thoroughly analyzed both influential parameters over a period exceeding five years of operation.

Table 3 illustrates the annual average of daily aggregations for both parameters and Y_{ref}, including their five-year average and CIs. We computed the daily T_{amb} by averaging the data collected during daylight hours, and we calculated the daily APE weighted by the corresponding irradiance. Our findings indicate a decline in Y_{ref} during the initial years,

Table 3
Annual average of daily aggregated climatic parameters (Y_{ref}, T_{amb}, APE): Per twelve-month period from Mar-2019 to Feb-2024 and the total average (5-year) including the confidence interval.

Site-specific features	First year	Second year	Third year	Fourth year	Fifth year	5-year average and CI
$\boldsymbol{Y_{ref}}$ (kWh/kW/day)	3.95	3.92	3.71	4.26	4.43	**4.08** [3.99, 4.18]
Diurnal $\boldsymbol{T_{amb}}$ (°C)	19.36	18.76	18.34	18.43	21.86	**19.44** [19.29,19.6]
APE (eV)	1.925	1.917	1.918	1.914	1.921	**1.917** [1.916,1.917]

followed by an increase in the final two years, culminating in an average of 4.08 kWh/kW/day across the five years. The annual trends of Y_{ref} positively correlate with those of T_{amb}. As anticipated, the measured diurnal T_{amb} exhibitis an annual average of about 19.44 °C, below yearly temperatures generally observed in hot deserts globally [19]. The spectral distribution, represented by the APE, maintains an almost consistent average of approximately 1.92 eV despite transitioning the spectroradiometer from the POA to the horizontal plane in 2023. This observation contributes to a broader, long-term understanding consistent with the findings reported by Conde et al. (2021) [39] and Sevillano-Bendezú et al. (2022) [25]. Lima exhibits a blue-shifted spectral distribution over the recording period, primarily due to its low latitude, as Sevillano-Bendezú et al. (2023) [24] indicated. Fig. A.1 in Appendix A outlines the Y_{ref}, T_{amb}, and APE trends over different time aggregations.

3.1.1. Module temperature effects on PV performance

Fig. 4 illustrates the influence of T_{mod} variations on the MPR for each of the eight PV modules represented by $\Delta MPR_{temperature}$. It also delineates the seasonal fluctuations of the Y_{ref} and T_{amb}. An examination of the data reveals that the trends of the Y_{ref} and T_{amb} exhibit a noteworthy similarity, albeit with irregular temporal shifts. Furthermore, both parameters demonstrate distinct seasonality, characterized by peak values during the summer months and troughs in the winter. The c-Si-based PV solar devices generally demonstrate higher γ compared to thin-film PV devices [40]. Both γ and T_{mod} significantly influence $\Delta MPR_{temperature}$. Consequently, the γ s listed in Table 2, when analyzed in conjunction

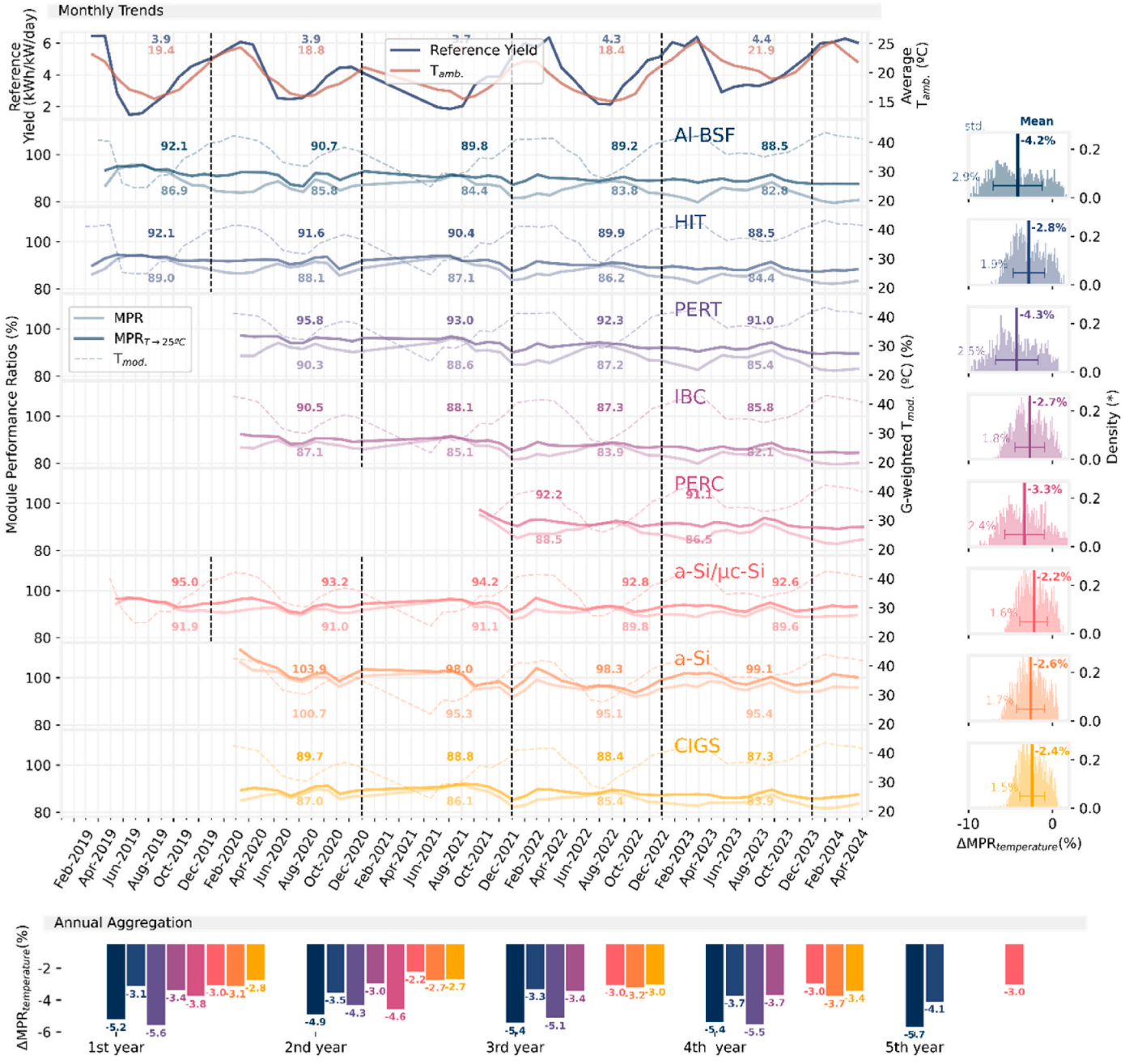

Fig. 4. Monthly trends of MPR before (MPR) and after temperature correction ($MPR_{T\to25°C}$) along with the average T_{mod}. Numbers above the lines represent the annual $MPR_{T\to25°C}$ and below, the annual MPR. Additionally, the Y_{ref} and the monthly averaged ambient temperature (T_{amb}) are shown. Right side: Histograms of the daily $MPR_{T\to25°C}$ and MPR differences ($\Delta MPR_{temperature}$). The mean and standard deviation (std) representing the average losses due to T_{mod} variations and its spread are plotted. In the bottom: $\Delta MPR_{temperature}$ of the annual aggregation for each consecutive year of monitoring.

with the average T_{mod}, provide a meaningful framework to explain the disparities in average $\Delta MPR_{temperature}$ across the various PV modules. The Al-BSF and PERT modules exhibit the most substantial losses among the c-Si modules, while the PERT module marginally surpasses the Al-BSF module. We attribute this observation to the PERT increased T_{mod}, as indicated in Table 4, which notably exceeds expectations based solely on the opposing effects of γ s shown in Table 2. The PERC module presents a higher absolute γ compared to PERT. Conversely, the average T_{mod} demonstrates the opposite and prevailing influence on $\Delta MPR_{temperature}$. HIT and IBC modules benefit from smaller absolute γ s among their c-Si module counterparts, leading to the smallest average $\Delta MPR_{temperature}$. In contrast, the diminished absolute γ of thin-film PV modules results in a comparatively more minor absolute $\Delta MPR_{temperature}$. Furthermore, the increased average T_{mod} in a-Si and CIGS technologies contribute to a higher loss in $\Delta MPR_{temperature}$ relative to the a-Si/μc-Si configuration. The seasonality of $\Delta MPR_{temperature}$ exhibits an inverse relationship with the seasonality of T_{mod} and is proportional to the standard deviation (std) observed in the corresponding histograms. Notably, the Al-BSF and PERT modules demonstrate the most significant losses and seasonal variations compared to others. In contrast, the IBC and HIT modules report the lowest fluctuations among mono-Si PV modules. For the thin-film PV modules, the impact of T_{mod} appears to remain relatively consistent across the different types. Additionally, Fig. 4 presents the annual aggregated $\Delta MPR_{temperature}$, which tends to exceed the average values of daily aggregations. This discrepancy can be attributed to the arithmetic nature of calculating the simple average of daily $\Delta MPR_{temperature}$. Nevertheless, the overall trends appear to be consistently maintained.

3.1.2. Solar spectrum variation influences on PV performance

Fig. 5 illustrates the monthly trends of spectral effects on the MPR via the $\Delta MPR_{spectrum}$. The APE exhibits limited seasonality, predominantly attributable to the low latitude, as observed by Sevillano-Bendezú et al. (2023) [24]. The mono-Si modules indicate spectral losses ranging from −0.7 % to −1.5 %, with the HIT PV module demonstrating the most significant losses, indicating heightened sensitivity to spectral variations. Conversely, the IBC module experiences the least daily influences. Among the thin-film PV technologies, the CIGS PV module is subject to relatively minor spectral variations, revealing daily losses of −0.6 %. Notably, the a-Si module shows average daily gains of 5.7 %, outperforming and reversing the trend of the other technologies. Despite changes in the inclination plane from 15° to horizontal in 2023, APE and SMM maintain consistent daily trends over time. This constancy is likely due to the optimal inclination angle being minimal at low latitudes, thereby rendering the change in spectral distribution insignificant on a horizontal plane. The annual aggregations of $\Delta MPR_{spectrum}$, depicted in the bottom of Fig. 5, are approximately aligned with the average values of daily aggregations, indicating a strong similarity of the calculation methodologies for daily and annual averages, in contrast to the aggregations in $\Delta MPR_{temperature}$. Fig. A.2, A.3, and A.4 outline the trends under various aggregation periods—daily, weekly, monthly, and annual—of MPR, $MPR_{T\to 25^{\circ}C}$, and $MPR_{T\to 25^{\circ}C}^{G_{\lambda}\to AM1.5G}$, respectively. Table A.1 in Appendix A summarizes the annual aggregated MPRs for each PV module across all analyzed years. Notably, the MPR of the a-Si PV module surpasses 100 %. This phenomenon is mainly attributable to the spectral gains exhibited by this module, particularly under Lima's blue-shifted spectrum.

3.2. Long-term PV module performance comparison

PV modules in the field are continuously subject to both intrinsic and extrinsic effects throughout their operational lifespan. An estimate of these influences is essential for conducting a long-term comparative analysis of PV modules. This study relies on the PLR to capture these effects.

3.2.1. PLR analysis

Fig. 6 depicts the MPI-based PLR utilizing various statistical methods throughout the entire recording period, including partial years. MPI enables the definition of PLR concerning several performance parameters, namely power output, V_{oc}, I_{sc}, and FF. Fig. 6(a) shows the power-based PLR. We added PLR based on the P_{nom} metric and the OLS approach to serve as a reference and exemplary pipeline based on a dissimilar metric. Notably, despite the inherent differences among the PLRs, significant overlap in the CIs often occurs, indicating the feasibility of integrating various performance-related methodologies to derive the consolidated $\overline{PLR}$ [13]. Across all evaluated cases, the CSD methodology exhibits a relatively narrow CI, primarily influenced by the interpolation performed to deal with missing data, particularly for this statistical method. The YoY method showed robustness and accuracy within linear statistical methods [11]. In this study, the YoY method yields the most extensive CI, effectively capturing a broad spectrum of losses that do not fit a single linear regression. This discrepancy is particularly pronounced for the a-Si module, where the YoY and OLS CIs suggested statistically distinguishable PLRs. Moreover, data availability presents a critical consideration, as evidenced by the PERC module, which shows a pronounced increase in CI, attributable to the limited dataset encompassing only 2.6 years of observations. To report a comparative PLR effectively, we adopt the ensemble approach, which integrates metrics of MPR, MPI, and P_{nom} as the three relevant metrics alongside the three statistical methodologies of OLS, YoY, and CSD. This comprehensive strategy encompasses a total of nine distinct analytical pipelines, which will be presented in the subsequent subsection.

Fig. 6(b), (c), and (d) illustrate the PLRs for V_{oc}, I_{sc}, and FF, respectively. We apply the three statistical methods to analyze each parameter: OLS, YoY, and CSD. The PLRs for V_{oc} hover around zero, typically ranging from −0.5 % to 0.4 %. In contrast, the PLRs for I_{sc} and FF exhibit a broader spectrum of variation, which is especially significant for I_{sc}. These observations are consistent with the underlying physics of PV modules and their degradation mechanisms. V_{oc} is primarily governed by the intrinsic properties of the cells, such as the semiconductor material's bandgap and the quality of the active junction region. This fundamental dependence, coupled with its logarithmic relationship to current, inherently renders V_{oc} less susceptible to certain degradation factors [41]. Consequently, the narrow range of V_{oc} PLRs suggests that these electrical characteristics and the integrity of charge separation would persist over the observed period, withstanding potential extrinsic influences such as minor increases in surface or interfacial recombination. Conversely, I_{sc} is directly proportional to the number of absorbed photons and the efficiency of charge carrier collection [42]. Thus, I_{sc} stems highly susceptible to external factors, such as soiling, encapsulant discoloration, and any internal defects that reduce the active area or hinder carrier collection, leading to more pronounced performance losses. Similarly, FF is a strong indicator of the module's overall electrical integrity. Its PLR is often influenced by a combination of other losses, particularly being highly sensitive to increases in series resistance due to factors such as degrading interconnects and solder joints, as well

Table 4
Irradiance-weighted T_{mod} over complete years of operation.

	Al-BSF	HIT	PERT	IBC	PERC	a-Si/μc-Si	a-Si	CIGS
G-weighted T_{mod} (°C)	36.05	36.55	36.77	35.70	34.89	35.18	36.17	36.51

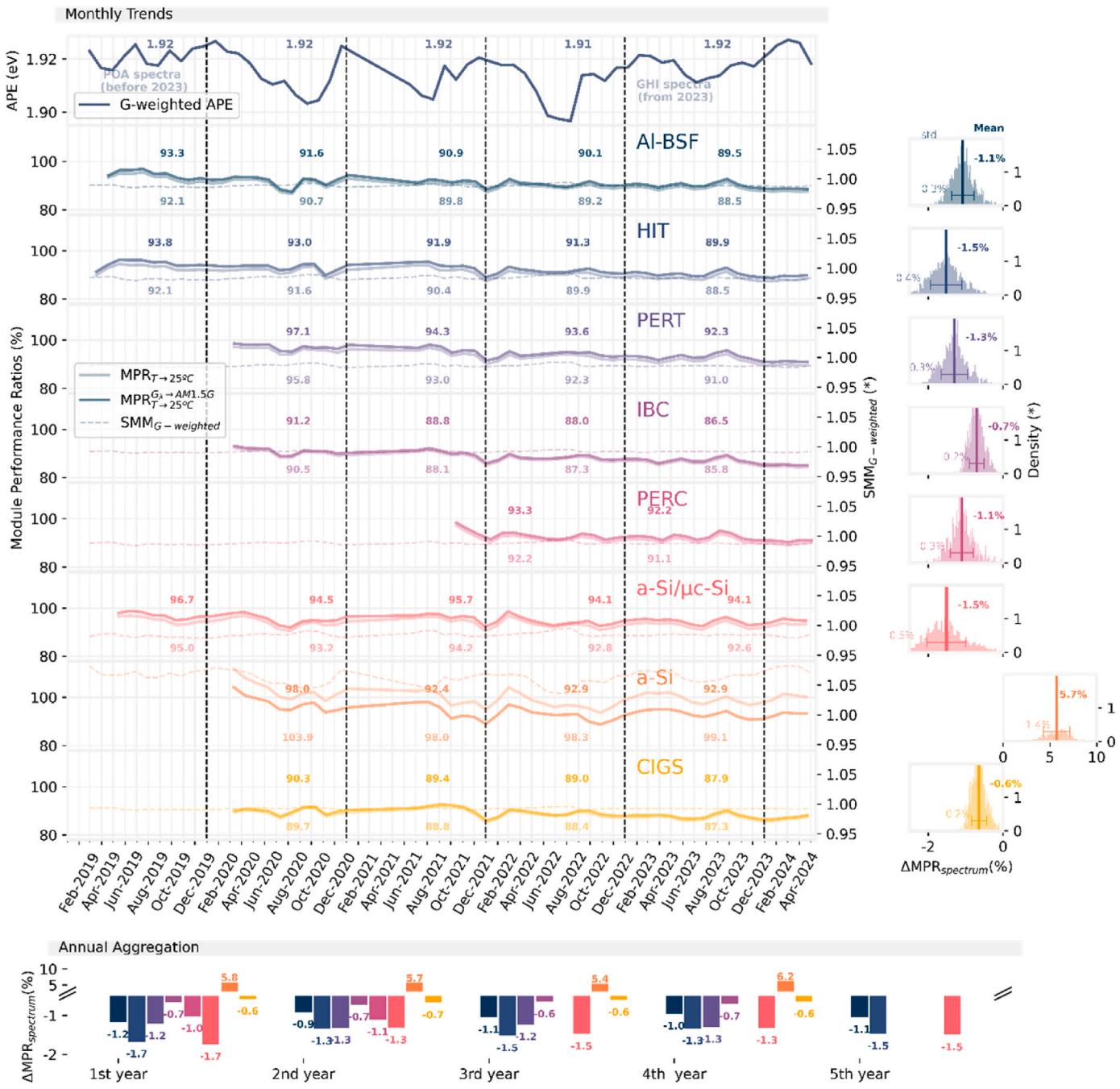

Fig. 5. Monthly MPR trends corrected by temperature ($MPR_{T\to25°C}$) and after spectrum and temperature correction ($MPR^{G\to AM1.5G}_{T\to25°C}$) along with the monthly irradiance-weighted Spectral Mismatch Factor ($SMM_{G\text{-}weighted}$). Numbers above the lines represent the aggregated annual $MPR^{G\to AM1.5G}_{T\to25°C}$, and below, the aggregated annual $MPR_{T\to25°C}$). Additionally, we include the irradiance-weighted APE ($APE_{G\text{-}weighted}$) with histograms of the daily $MPR^{G\to AM1.5G}_{T\to25°C}$ and $MPR_{T\to25°C}$ differences ($\Delta MPR_{spectrum}$). The mean and standard deviation representing the average spectral losses and its spread are plotted. In the bottom, $\Delta MPR_{spectrum}$ of the annual aggregation for each year.

as decreases in shunt resistance from the formation of leakage paths [43].

Within this narrow range of V_{oc} variation, the IBC module notably exhibits the highest losses, recording a PLR of about −0.5 %. This higher PLR for V_{oc} in IBC modules might be due to the sensitivity of their sophisticated rear-contact passivation layers to long-term field exposure. Its PLR for I_{sc} remains around −1 %, similar to most other modules, and the FF appears stable, with no significant losses or gains over time [44]. Conversely, the CIGS module shows slight improvements in V_{oc} across all three statistical methods and minimal FF losses. These V_{oc} increases are typical of certain thin-film technologies, often due to beneficial light-induced stabilization effects [45]. However, its PLR for I_{sc} is more negative than that of the other modules. This may suggest a greater vulnerability to degradations and losses that affect charge collection pathways in the CIGS device structure [46].

Furthermore, the FF losses observed in the PERT module are comparable to those in a-Si. The typical bulk properties degradations of a-Si anticipate an increase in defects, which would adversely affect the FF by diminishing shunt resistances in the cells [47]. Conversely, for the PERT module, where bulk material properties are usually highly optimized for

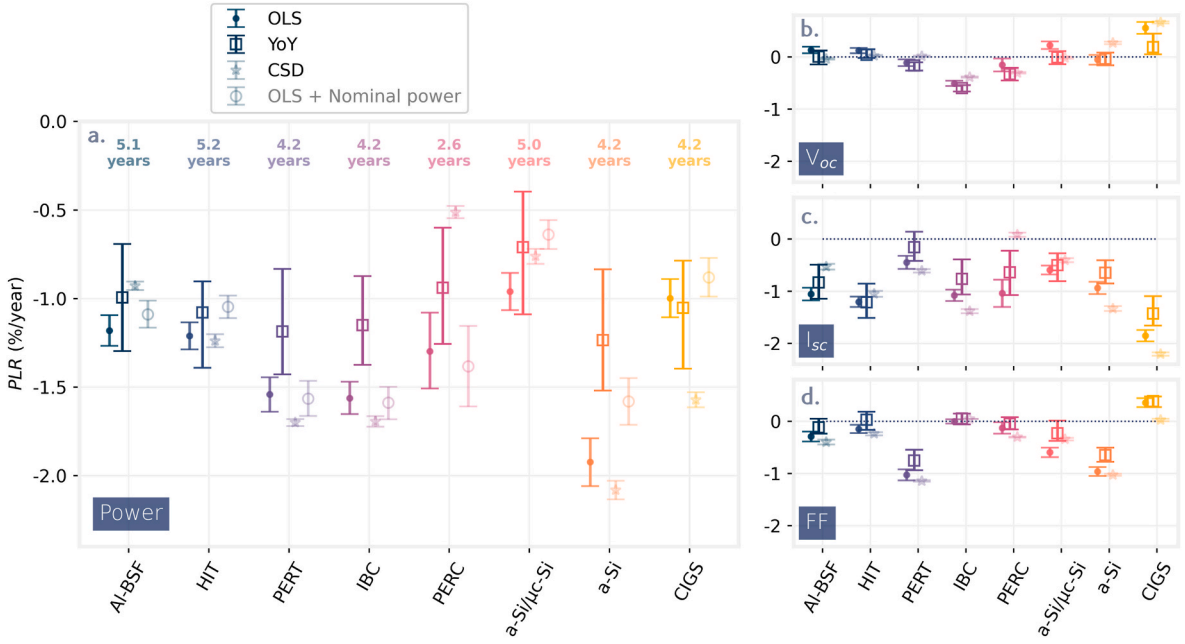

Fig. 6. MPI-based PLRs using the OLS, YoY, and CSD methods for the (a) power (including results from an additional pipeline taking into account the experimental nominal power adjusted by the SMM along with the OLS method, labeled in legend as: OLS + Nominal power) (b) V_{oc}, (c) I_{sc} and (d) FF. Marker and whiskers indicate median and CI, respectively.

efficiency, the observed PLR of FF may mainly be affected by an increase in series resistance or a decrease in shunt resistance over time. Electroluminescence images, while not presented here, did not reveal correlative evidence with these observations. A more thorough investigation into these phenomena necessitates a forensic analysis, which exceeds the constraints of the current study.

3.2.2. *PV module benchmarking*

This subsection aims to synthesize the results within the context of a benchmarking application.

The comparative table in Fig. 7 outlines key performance features of different PV modules, showing their nameplate efficiency, the average daily aggregated MPR over four complete years of operation (4-y MPR), except for the PERC module, which considers only two complete years of data for the 4-y MPR calculation, and the main factors causing losses in

Benchmarking mid-term PV module performance

5+ years of measured data

Modules	Rated Efficiency (%)	4-y MPR | CI (%)	$\Delta MPR_{temperature}$ | CI(%)	$\Delta MPR_{spectrum}$ | CI(%)	Approx. ΔMPR_{others} (%)	$\overline{PLR}$ | CI(%/year)
5+ years Al BSF	16.5	**86.76** [86.51, 87.02]	**-4.16** [-4.31, -4.00]	**-1.08** [-1.10, -1.07]	**-5.8**	**-0.99** [-1.04, -0.94]
5+ years HIT	19.7	**88.68** [88.50, 88.88]	**-2.84** [-2.94, -2.73]	**-1.53** [-1.55, -1.50]	**-4.5**	**-1.13** [-1.18, -1.09]
4+ years PERT	20.1	**89.14** [88.89, 89.40]	**-4.27** [-4.42, -4.11]	**-1.30** [-1.33, -1.28]	**-1.3**	**-1.61** [-1.64, -1.58]
4+ years IBC	21.4	**85.37** [85.17, 85.57]	**-2.71** [-2.82, -2.61]	**-0.71** [-0.72, -0.69]	**-7.4**	**-1.59** [-1.64, -1.55]
2+ years PERC	19.3	**88.50** [88.23, 88.78]	**-3.33** [-3.52, -3.14]	**-1.11** [-1.13, -1.08]	**-5.8**	**-0.90** [-0.98, -0.83]
5+ years a-Si/µc-Si	9.0	**91.80** [91.63, 91.97]	**-2.24** [-2.32, -2.15]	**-1.51** [-1.54, -1.49]	**-2.8**	**-0.69** [-0.75, -0.62]
4+ years a-Si	6.3	**97.22** [96.99, 97.48]	**-2.63** [-2.72, -2.52]	**5.72** [5.64, 5.81]	**-2.7**	**-1.30** [-1.38, -1.22]
4+ years CIGS	14.3	**85.92** [85.76, 86.08]	**-2.44** [-2.53, -2.35]	**-0.65** [-0.66, -0.63]	**-8.4**	**-1.07** [-1.13, -1.01]

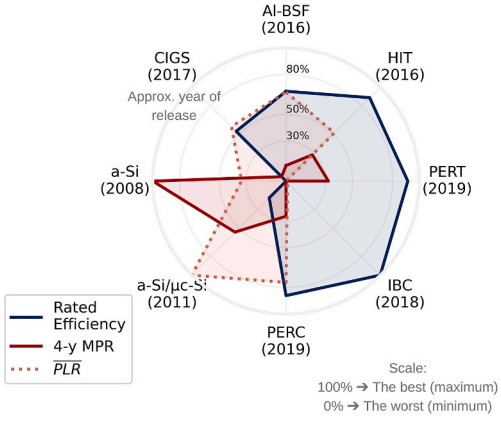

Fig. 7. Benchmarking mid-term PV module performance in daily aggregation. The table columns detail the 4-year MPR (measured over the first four complete years, except for PERC), the $\overline{PLR}$ in %/year (calculated using the entire available dataset, including incomplete years), and the derived performance losses ($\Delta MPR_{temperature}$, $\Delta MPR_{spectrum}$, and ΔMPR_{others}), which were determined using all of the maximum available complete years. The radar chart on the right visually compares the Nominal Efficiencies, 4-year MPRs, and $\overline{PLR}$ s on a relative scale.

PV performance. The daily average $\Delta MPR_{temperature}$ and $\Delta MPR_{spectrum}$ encompass only complete years (all available) to reflect climatic impacts over time better, mitigating potential seasonal bias.

The $\overline{PLR}$ derived from the ensemble approach provides a singular average value based on nine different PLR pipelines (see Fig. A.11 in Appendix A). We applied a similar procedure to estimate representative CIs. Intriguingly, the loss factors we examined align well with the annual aggregated MPR after correcting for losses in both the first and last complete years of operation, as illustrated in Fig. A.5 in Appendix A. This alignment indirectly validates this study's methodology.

Incorporating loss corrections for each year of operation allowed for identifying consistent average annual residual losses, designated as ΔMPR_{others} and included in the comparative table in Fig. 7. These losses appear relatively stable and capture additional factors affecting PV performance not explicitly addressed within this study, such as low irradiance effects, angular losses, seasonal soiling accumulation, shadings, and undetected malfunctions [48]. Decoupling the various influences on ΔMPR_{others} is challenging due to the site-specific complexities of each of the remaining loss factors exhibited. Developing a precise statistical estimation of these influences extends beyond the confines of the present research.

The radar chart in Fig. 7 illustrates the relative comparison of two primary performance metrics, 4-y MPR, and the $\overline{PLR}$, alongside rated efficiency. These metrics are normalized on a scale from 0 % to 100 %, wherein a score of 0 % indicates the lowest efficiency, performance, and most negative $\overline{PLR}$. In comparison, 100 % signifies the module with the highest efficiency, 4-y MPR, and the least negative $\overline{PLR}$. We labeled each PV module with its approximate year of release, as inferred from the corresponding datasheet.

ΔMPR s and $\overline{PLR}$ extend up to the maximum of complete available years and the entire dataset (including incomplete years), respectively. Notably, the PERC module is limited by only 2.6 years (or two complete years). 4-y MPR establishes the boundaries for comparing the modules' performance within a similar period of outdoor exposition. Conversely, $\overline{PLR}$ introduces a perspective of long-term performance, assuming that performance losses will exhibit a linear behavior over the module's operational lifespan.

The a-Si module reveals the highest 4-y MPR, getting closer to 100 %. This phenomenon can be attributed to the significant spectral gains discussed earlier. Moreover, the a-Si module demonstrates a $\overline{PLR}$ of −1.3 %/year, which is considerably high among the modules studied. This module is also the least efficient and oldest, according to its approximate year of release. Although the a-Si/μc-Si-based module has the second-lowest nameplate efficiency, it registers the best $\overline{PLR}$ among the studied modules, contributing to its high 4-y MPR of 91.8 % and making it the most conservative in efficiency and performance across the four years.

The CIGS module is observed to have the second-lowest 4-y MPR relative to the studied modules. Data illustrate that it carries the highest estimated residual losses, a factor that significantly contributes to its diminished 4-y MPR. While exhibiting the lowest nameplate efficiency among c-Si modules, the Al-BSF module has the best $\overline{PLR}$, excluding the PERC module, which maintains an optimistic $\overline{PLR}$ influenced by its shortest exposure time relative to the other modules.

The IBC module features the highest nameplate efficiency; however, it records the lowest 4-y MPR, and its $\overline{PLR}$ is among the worst, similar to that of the PERT module, notably impacted by associated remanent losses. The HIT module ranks third in nameplate efficiency, achieving a value of 19.7 %, with a commendable $\overline{PLR}$ of −1.13 %/year, marking it as one of the leading performers among the mono-Si PV modules. Table A.2 in Appendix A complement this analysis by incorporating the expected Y_{mod} for each PV technology.

To contextualize our results, we compared the ensemble $\overline{PLR}$ s against established global benchmarks for long-term PV degradation. The established literature median for c-Si technologies is −0.5 to −0.6 %/year, as reported in Jordan et al. (2016) [49]. Our c-Si modules (Al-BSF, HIT, PERT, IBC) showed $\overline{PLR}$ s ranging from −0.90 %/year (PERC, noted as optimistic due to short duration) to −1.61 %/year (PERT), generally exceeding this median, but remaining within the expected range for non-accelerated degradation, especially considering the global mean c-Si degradation is $\leq$ −0.9 %/year [49]. Notably, our HIT module $\overline{PLR}$ aligns closely with the reported global ~1 %/year average for its technology. For thin-film technologies, our results are consistent with the reported rates exceeding −1 %/year, specifically a-Si (−1.3 %/year) and CIGS (−1.1 %/year). However, our a-Si/μc-Si module shows a remarkably low $\overline{PLR}$ of −0.69 %/year. The overall slightly elevated $\overline{PLR}$ s could be associated with Lima's high humidity, high UV, and ambient temperature combination, which could impact degradation. Furthermore, our methodology adheres to the IEA PVPS Task 13 framework for minimizing inaccuracies and providing consistent PLR estimates [12].

3.2.3. Example: projected performance over a 25-year horizon

To offer a valuable comparative assessment of PV module technologies, we project their estimated long-term performance over a 25-year horizon. This assessment quantifies the useful energy percentage over 25 years to benchmark the suitability of the module. We derive this percentage in Equation (B.8) of Appendix B. It is crucial to note that accurately modeling long-term Performance Loss Rates (PLR) involves inherent complexities; therefore, we detail the significant simplifying assumptions underpinning this projection in Appendix B. Consequently, this rough estimate should be treated cautiously, serving as a rule of thumb rather than an exact quantitative result.

Utilizing this approach and inputs from the comparative table in Fig. 7, our estimates indicate that the HIT module would utilize approximately 15 % of the incident cumulative irradiation over 25 years of operation as seen in Table A.3 in Appendix A. The IBC module follows closely with an estimated utilization of 14.6 %, PERT at 14.5 %, and Al-BSF at 12.5 %. Notably, PERC demonstrated an enthusiastic utilization figure of 15 %, but we should be cautious in interpreting this result since mainly its $\overline{PLR}$ comes from a shorter examination period.

Therefore, under this simplified approximation, the 2016 HIT module appears to outperform both the 2018 IBC and 2019 PERT modules in terms of performance. Furthermore, the thin-film PV modules, specifically a-Si, CIGS and a-Si/μc-Si, reported utilization percentages of 5.3 %, 10.6 %, and 7.6 %, respectively. Using a similar approach, we estimate the MPR after 25 years of operation and its expected actual efficiency. Table A.4 in Appendix A summarizes all these estimates and the above results. We validated this approach by predicting the annual aggregated MPR for a specific year of operation, as detailed in Table A.3 in Appendix A. The results indicate an absolute error of less than 1 %.

A more robust estimate would consider accurate models for long-term PLR behavior over the lifespan of the PV modules. Additionally, it is imperative to contrast the results in economic terms, a consideration that extends beyond the current analysis.

4. Conclusions

We conducted a long-term performance assessment of Al-BSF, HIT, PERT, IBC, PERC, a-Si/μc-Si, a-Si, and CIGS PV modules in Lima, a subtropical, desertic, and low latitude site. This analysis involved the calculation of different performance metrics, the primary factors being MPR and PLR. We represent climatic influences on performance as $\Delta MPR_{temperature}$ and $\Delta MPR_{spectrum}$, which are related to the variation of T_{mod} and spectral distribution, respectively. We report that the γ and the T_{mod} play an important role when comparing $\Delta MPR_{temperature}$ among the different PV technologies. Conversely, c-Si PV modules tend to exhibit a higher $\Delta MPR_{temperature}$ than thin-film PV modules, mainly motivated by the influence of the γ. However, such trends within the two groups of

modules can be reversed due to the influence of T_{mod}. Among the c-Si PV modules, the PERT module exhibited the largest influence on $\Delta MPR_{temperature}$ of around −4.3 %, while IBC exhibited a low −2.7 %. The spectral influence represented by $\Delta MPR_{spectrum}$ remained between −0.7 and −1.5 % for the c-Si modules. However, among the thin-film PV modules, the a-Si module proved to reverse the trend of the other technologies by demonstrating a gain of 5.7 %, outperforming in absolute value the spectral influences of the other modules. We analyzed the PLR for different performance parameters, including the power output, V_{oc}, I_{sc}, and *FF*. Overall, the losses in V_{oc} were minimal, typically staying above −0.5 % and below 0.4 %. In contrast, I_{sc} demonstrated a wider range of degradation, with CIGS values approaching nearly −2.0 %. Meanwhile, the losses in FF were unexpectedly more significant for the PERT module, and comparable with the a-Si module. Using nine different PLR pipelines allowed us to apply the ensemble approach to obtain a single and reliable PLR. The c-Si PV modules demonstrated PLRs between −0.9 and −1.6 %/year. The PERC module had the lowest value, but the brief exposure time relative to the other modules contributed to the optimistic PLR observed. Meanwhile, the PERT module presented the most negative PLR. Benchmarking the ensemble PLRs showed that our c-Si module results generally exceed the global median of −0.5 to −0.6 %/year, suggesting that Lima's unique combination of high humidity and intense UV radiation may have a detrimental effect that accelerates degradation processes. The detailed analysis of the loss factors, including residual losses, enabled us to benchmark the performance of the eight PV modules. For this exercise, we roughly estimate the useful energy over 25 years of operation by significantly simplifying the complex behavior of PLR as a linear function of time. The HIT module, approximately released in 2016, achieved the highest score, delivering 15 % of useful energy from the cumulative irradiation over 25 years of operation, thus surpassing the 2018-IBC and 2019-PERT PV modules, which fell behind at 14.6 % and 14.5 %, respectively. In contrast, PERC obtained a high result of 15 %, influenced by its PLR, which is likely biased by the short study period. These benchmark results represent a broad technical study of the performance of different technologies for this particular site.

CRediT authorship contribution statement

Miguel Ángel Sevillano-Bendezú: Writing – review & editing, Writing – original draft, Visualization, Validation, Software, Methodology, Investigation, Formal analysis, Data curation, Conceptualization. **Luis Ángel Conde:** Writing – review & editing, Investigation, Data curation. **Michael Anthony García:** Writing – review & editing, Investigation. **José Rubén Angulo:** Writing – review & editing, Investigation, Data curation. **Juan de la Casa:** Writing – review & editing, Investigation, Formal analysis, Conceptualization. **José María Ripalda:** Writing – review & editing, Supervision, Investigation, Funding acquisition, Conceptualization. **Jan Amaru Töfflinger:** Writing – review & editing, Writing – original draft, Supervision, Resources, Project administration, Investigation, Funding acquisition, Formal analysis, Conceptualization.

Declaration of competing interest

The authors declare that they have no known competing financial interests or personal relationships that could have appeared to influence the work reported in this paper.

Acknowledgements

This work received financial support from PROCIENCIA through contract 124-2018-FONDECYT. J. A. Töfflinger acknowledges the financial support from the Vicechancellorship for Research (PI0997) of the Pontificia Universidad Católica del Perú. M. A. Sevillano-Bendezú and J. M. Ripalda acknowledge the AEI projects PID2021-124193OB-C22 (EU FEDER) and TED2021-130623B-I00 (EU PRTR). J. R. Angulo thanks the Vice-Rectorate for Research (VRI) of the Pontifical Catholic University of Peru for funding through the 2023 Postdoctoral Fellowship Support Program.

Appendix A

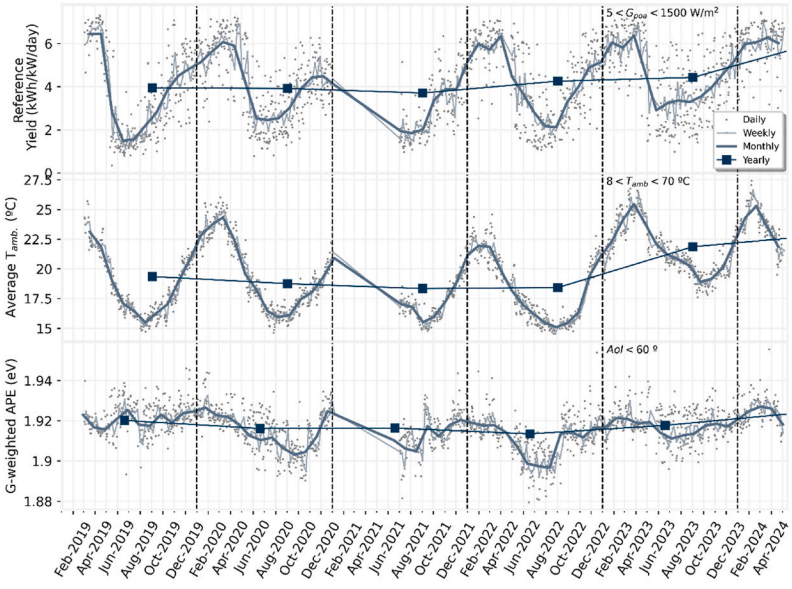

Fig. A.1. Time series of the Y_{ref}, average diurnal T_{mod}, G-weighted APE under different aggregations Daily, Weekly, Monthly and Yearly.

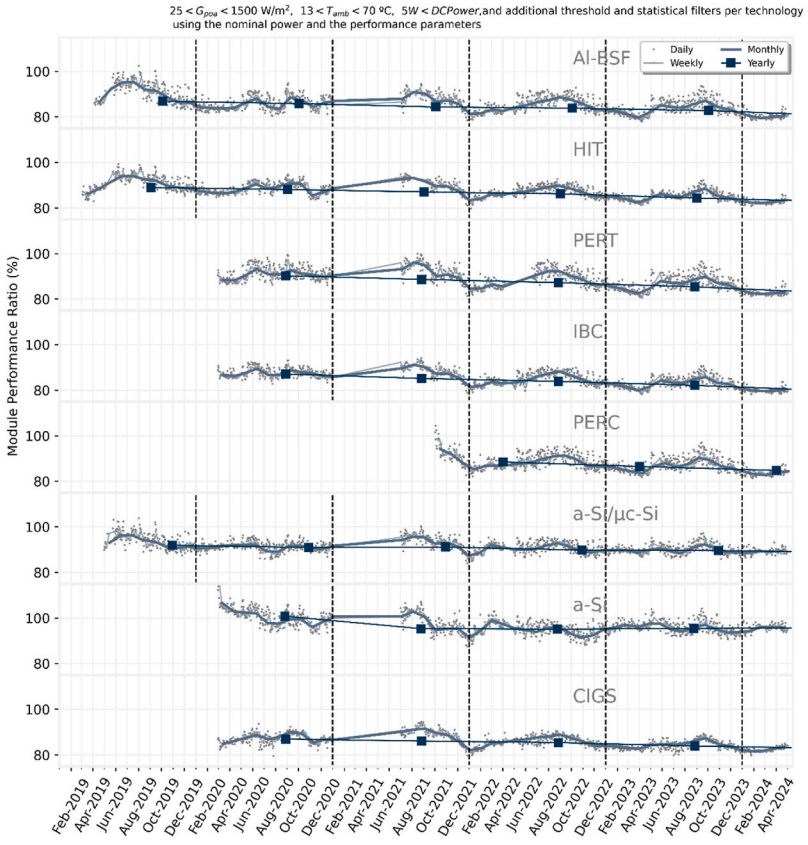

Fig. A.2. MPR under different aggregations Daily, Weekly, Monthly and Yearly for the eight PV modules.

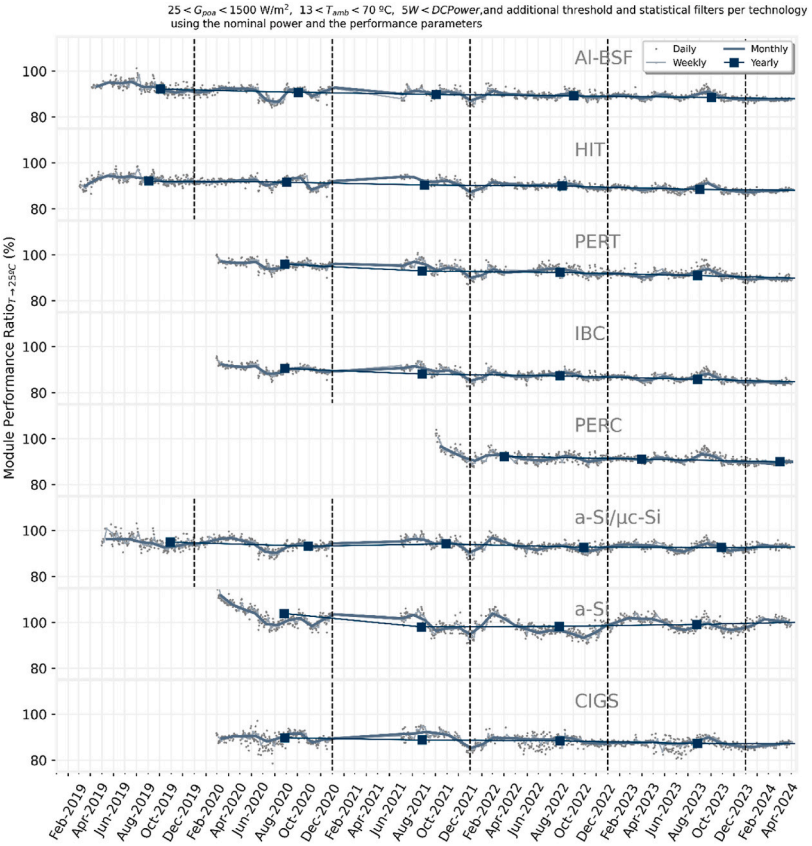

Fig. A.3. $MPR_{T\to25^{\circ}C}$ under different aggregations Daily, Weekly, Monthly and Yearly for the eight PV modules

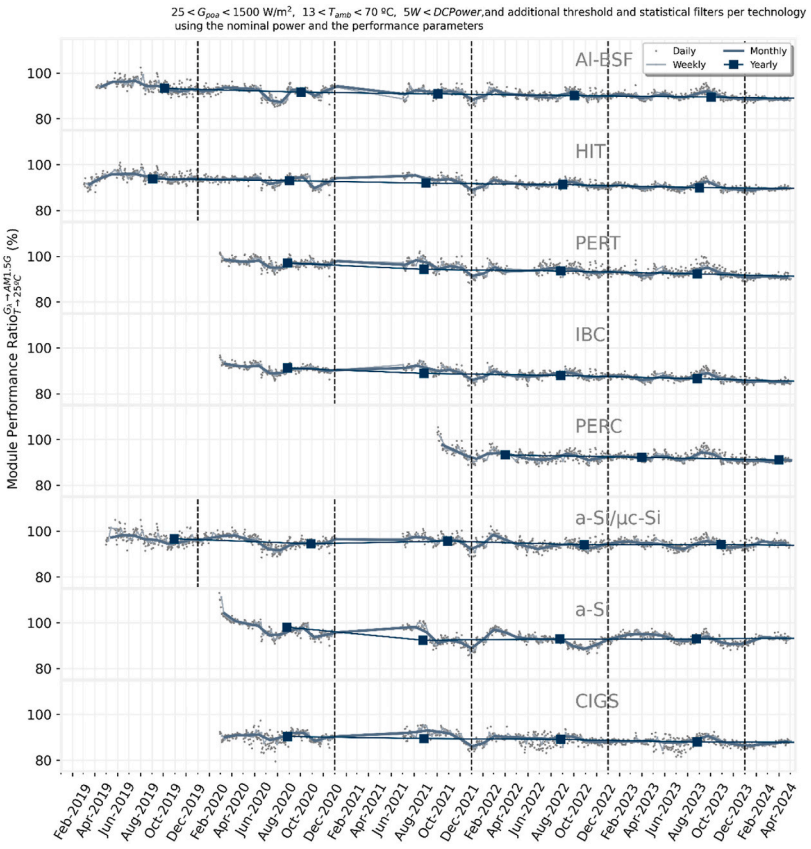

Fig. A.4. $MPR^{G\to AM1.5G}_{T\to 25^{\circ}C}$ under different aggregations Daily, Weekly, Monthly and Yearly for the eight PV modules

Table A.1
Annual MPR per year of operation for each PV module

Technology	Annual aggregated MPR (%)				
	First	Second	Third	Fourth	Fifth
Al-BSF	86.89	85.82	84.37	83.83	82.76
HIT	88.98	88.09	87.07	86.23	84.36
PERT	90.26	88.62	87.22	85.43	–
IBC	87.14	85.14	83.88	82.12	–
PERC	88.47	86.52	–	–	–
a-si/µc-Si	91.91	90.95	91.13	89.79	89.59
a-Si	100.75	95.29	95.07	95.36	–
CIGS	86.98	86.08	85.42	83.89	–

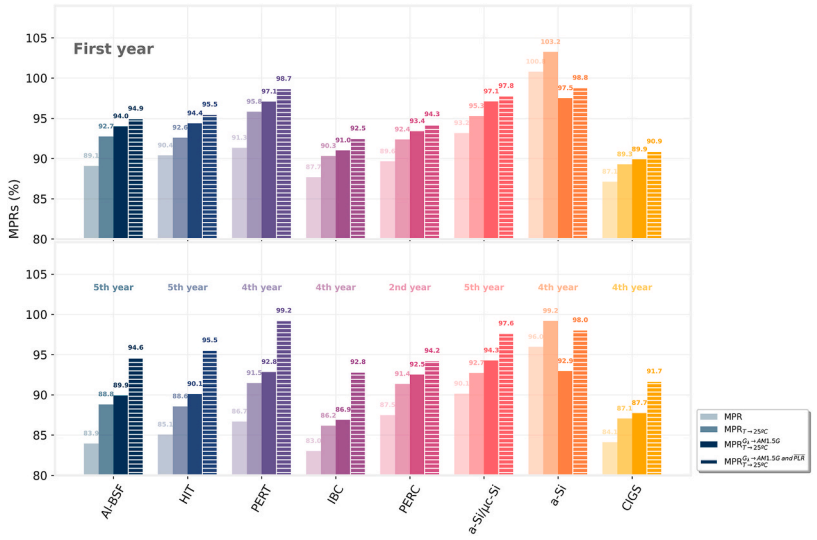

Fig. A.5. Modules performance ratios: MPR, $MPR_{T\to 25^{\circ}C}$, $MPR_{T\to 25^{\circ}C}^{G_{\lambda}\to AM1.5G}$, and MPR corrected by T_{mod}, SMM, and $\overline{PLR}$ ($MPR_{T\to 25^{\circ}C}^{G_{\lambda}\to AM1.5G\wedge\overline{PLR}}$). We assumed that the $\overline{PLR}$ produces a linear loss proportional to the year of operation.

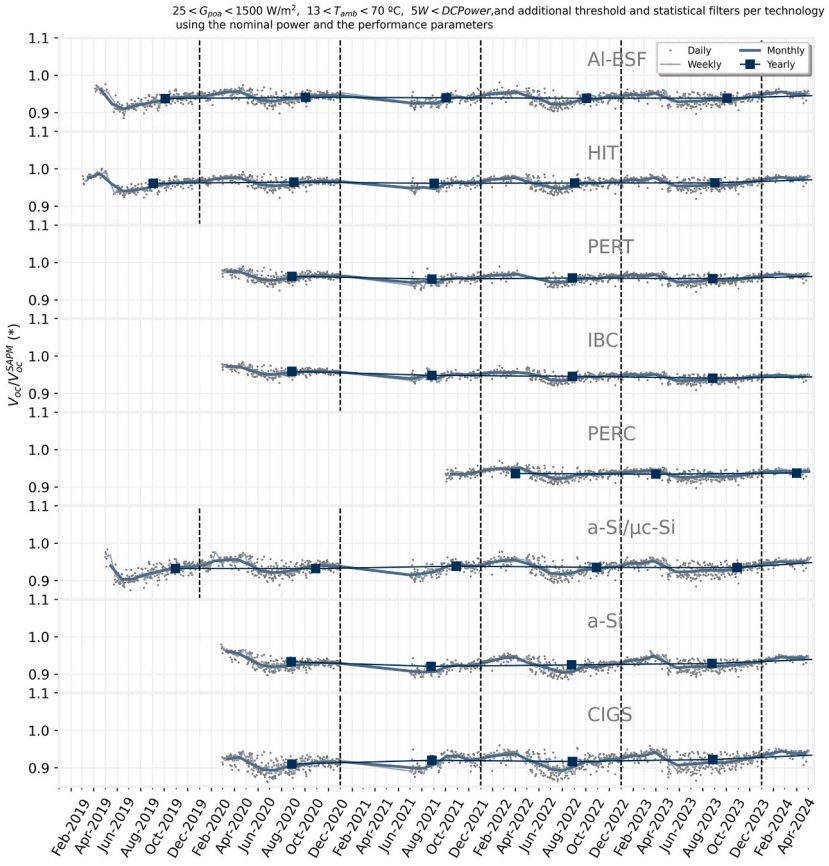

Fig. A.6. V_{oc} MPI under different aggregations: Daily, Weekly, Monthly and Yearly for the eight PV modules

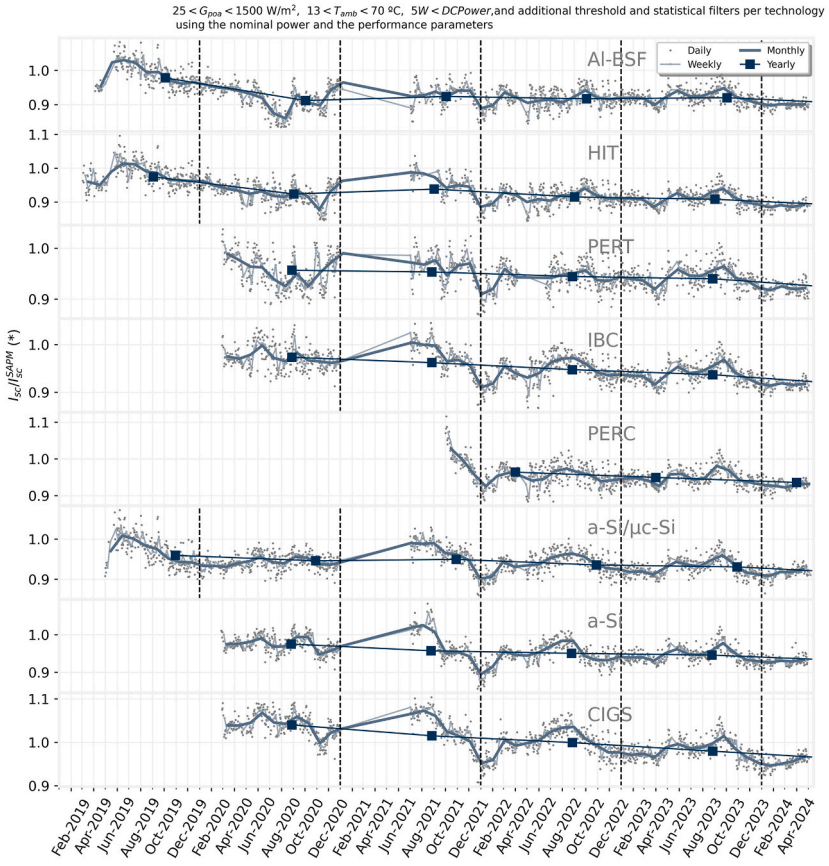

Fig. A.7. I_{sc} MPI under different aggregations: Daily, Weekly, Monthly and Yearly for the eight PV modules

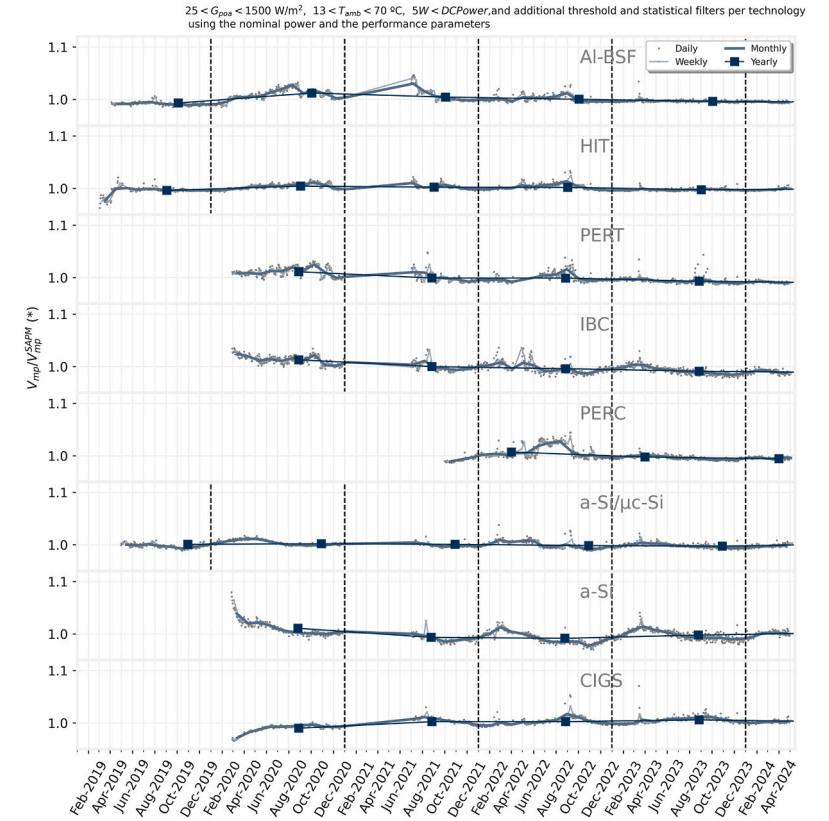

Fig. A.8. Voltage at maximum power point (V_{mp}) MPIunder different aggregations: Daily, Weekly, Monthly and Yearly for the eight PV modules

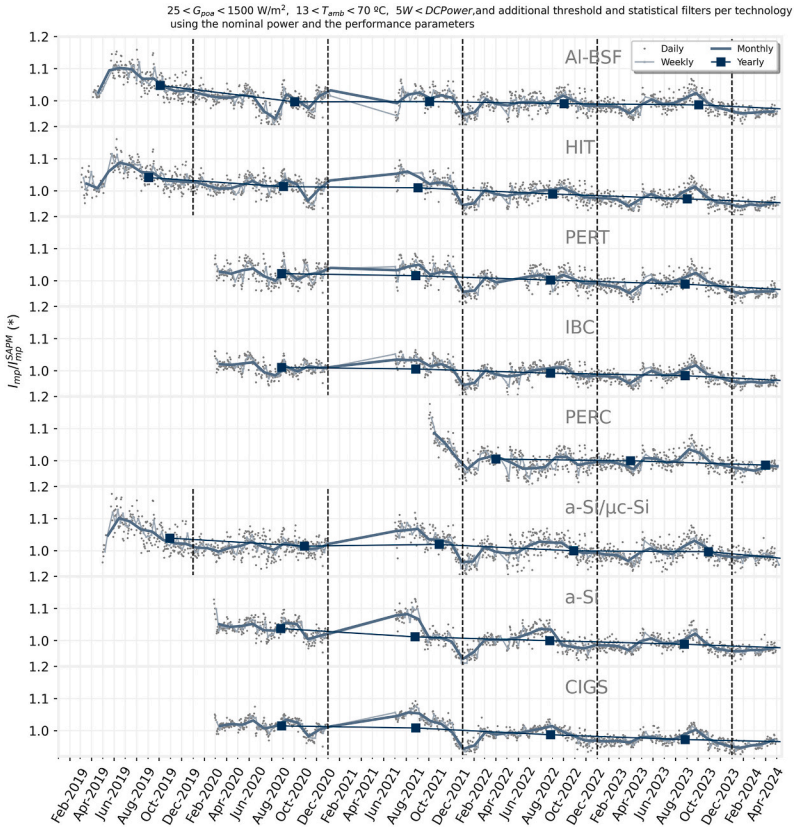

Fig. A.9. Current at maximum power point (I_{mp}) MPIunder different aggregations: Daily, Weekly, Monthly and Yearly for the eight PV modules

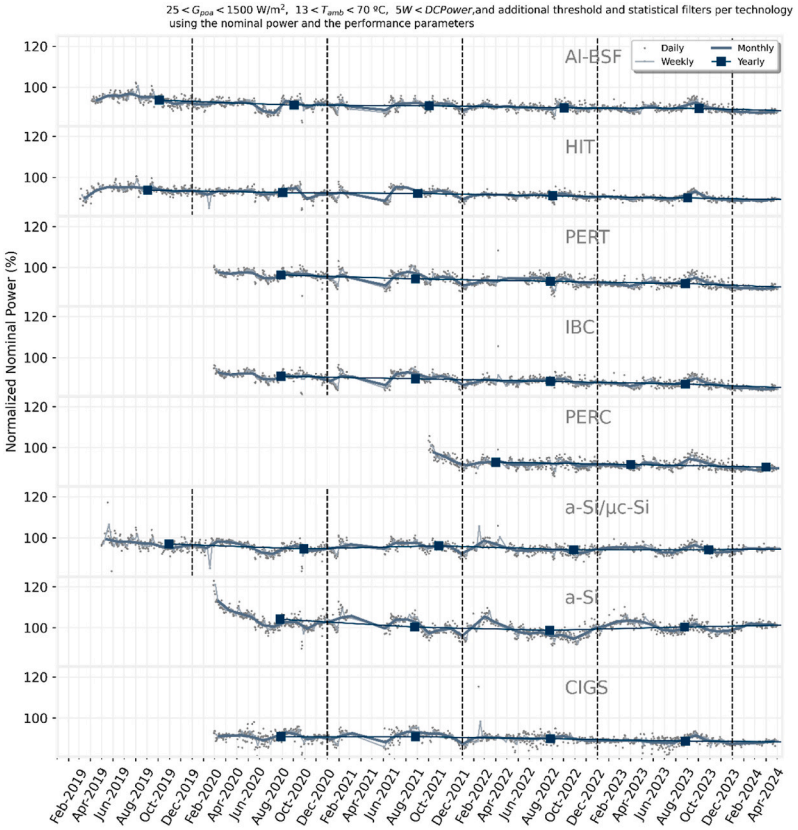

Fig. A.10. P_{nom} normalized to the nameplate power under different aggregations: Daily, Weekly, Monthly and Yearly for the eight PV modules

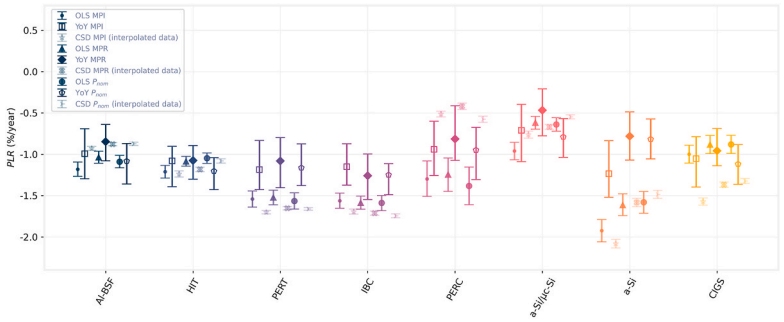

Fig. A.11. The nine PLR pipelines utilized to calculate the $\overline{PLR}$ for each PV module

Table A.2
Summary of key performance metrics: Y_{ref}, 4-y MPR, and estimated Y_{mod}. We calculated Y_{mod} by multiplying Y_{ref} times the 4-y MPR.

Tech	Only 4 years of data (Except for PERC which has only 2 complete years)					
	$\boldsymbol{Y_{ref}}$ (kWh/kW/day)		4-y MPR (%)		$\boldsymbol{Y_{mod}} = \boldsymbol{Y_{ref}} \times \boldsymbol{MPR}$, for 4 years (kWh/kWp/day)	
	Mean	CI	Mean	CI	Mean	CI
Al-BSF	4.02	[3.91,4.13]	86.76	[86.51,87.02]	3.49	[3.39,3.58]
HIT	4.03	[3.92,4.14]	88.68	[88.50,88.88]	3.57	[3.48,3.67]
PERT	4.13	[4.02,4.23]	89.14	[88.89,89.40]	3.68	[3.59,3.78]
IBC	4.13	[4.02,4.23]	85.37	[85.17,85.57]	3.52	[3.43,3.61]
PERC	4.25	[4.11,4.39]	88.50	[88.23,88.78]	3.77	[3.64,3.89]
a-Si/µc-Si	3.94	[3.83,4.05]	91.80	[91.63,91.97]	3.62	[3.52,3.72]
a-Si	4.07	[3.96,4.18]	97.22	[96.99,97.48]	3.96	[3.85,4.06]
CIGS	4.09	[3.99,4.20]	85.92	[85.75,86.08]	3.52	[3.43,3.61]

Table A.3
Approximate performance projections over 25 years of field exposition.

Tech (Approx. year of release)	Rated efficiency (%)	Estimate MPR after 25 years of operation (%)	Estimate Efficiency after 25 years of operation (%)	Approximate utilized energy over 25-years (%)
Al-BSF (2016)	16.5	64.10	10.58	12.54
HIT (2016)	19.7	62.74	12.36	15.04
PERT (2019)	20.1	52.86	10.63	14.50
IBC (2018)	21.4	49.27	10.54	14.64
PERC (2019)	19.3	66.85	12.90	15.00
a-Si/µc-Si (2011)	9.0	76.34	6.87	7.61
a-Si (2008)	6.31	67.84	4.28	5.27
CIGS (2017)	14.3	61.63	8.81	10.65

Table A.4
Validation of the approximate performance projection method by comparing annual aggregated MPR vs estimate annual MPR.

Tech	Years of operation	***MPR*** (%)	Estimate ***MPR*** (%)	Absolute error in estimating the ***MPR*** (%)
Al-BSF	5	83.95	83.91	0.04
HIT	5	85.05	85.43	0.37
PERT	4	86.68	86.62	0.06
IBC	4	83.02	82.72	0.30
PERC	2	87.48	87.65	0.17
a-Si/µc-Si	5	90.15	90.04	0.10
a-Si	4	95.96	95.13	0.83
CIGS	4	84.10	84.16	0.05

Appendix B

For this analysis, we primarily assume that the total annual irradiation of an arbitrary *i*-year of operation, $H_i = \overline{H} + \delta H_i$, experiences only slight variations from the average irradiation (i.e., $\delta H_i \ll \overline{H}$), and such deviations ($\delta H_i$) follow a quasi-normal distribution, so that, over *N* years of operation we can approximate:

$$\sum_{i=1}^{N} H_i \approx N\overline{H} \quad \text{B.1}$$

Furthermore, the energy generated in a particular *i*-year is estimated using the following expression:

$$E_i = H_i \times MPR_i \times \eta_{STC} \quad \text{B.2}$$

Where MPR_i represents the MPR for the *i*-year. MPR_i can be expressed as a function of the performance losses, namely, ΔMPR_i and PLR_i. For this study, we utilize the average ΔMPR and PLR as presented in the table in Fig. 7.

Modeling the effects of degradations over time is a complex task, as its behavior is frequently subject to nonlinearities. Given the inherent complexities in precisely describing long-term PLR behavior, and in an effort to provide a helpful comparative reference, we make a significant simplifying assumption, which should be applied with caution: linearly projecting the PLR over the system's lifetime (represented by $i \times PLR$), based on the data from over 5 years of operation demonstrated in the table in Fig. 7. With these assumptions we obtain the following expression for MPR_i:

$$MPR_i = 100\% + \Delta MPR + i \times PLR \quad \text{B.3}$$

Where ΔMPR is represented by the main performance losses in equation (B.4):

$$\Delta MPR = \Delta MPR_{temperature} + \Delta MPR_{spectrum} + \Delta MPR_{others} \quad \text{B.4}$$

From equation (B.2), the total energy produced over N years of operation can be estimated as:

$$\sum_{i=1}^{N} E_i = \eta_{STC} \times \sum_{i=1}^{N} H_i \times MPR_i \quad \text{B.5}$$

Substituting B.1 and B.3 into B.5 yields:

$$\sum_{i=1}^{N} E_i \approx \eta_{STC} \times \left\{ 100\% \times \sum_{i=1}^{N} \overline{H} + \sum_{i=1}^{N} \overline{H}[N \times \Delta MPR + i \times PLR] \right\} \quad \text{B.6}$$

By resolving the summations in B.6, expression B.7 is obtained:

$$\sum_{i=1}^{N} E_i \approx N \times \overline{H} \times \eta_{STC} \times \left\{ 100\% + \left[\Delta MPR + \left(\frac{N+1}{2} \right) \times PLR \right] \right\} \quad \text{B7}$$

From equation (B.6), the term within the brackets reflects the estimated effective percentage of energy output from a PV module over the *N* years of operation.

Finally, we derived equation (B.8) in accordance with the standard warranty duration typically provided by manufacturers, which is established at 25 years.

$$\textit{Useful energy percentage along 25-years} \approx \textit{Rated efficiency} \times (100\% + \Delta MPR + 13 \times PLR) \quad \text{B.8}$$

References

[1] N.M. Haegel, S.R. Kurtz, Global progress toward renewable electricity: tracking the role of solar (Version 4), IEEE J. Photovoltaics (2024) 1–9.

[2] H. Mirletz, S. Ovaitt, S. Sridhar, T.M. Barnes, Prioritizing circular economy strategies for sustainable PV deployment at the TW scale, EPJ. Photovoltaics 15 (2024) 18.

[3] M. Owen-Bellini, J.Y. Hartley, A. Jain, D.C. Jordan, L.T. Schelhas, T.M. Barnes, DuraMAT: building a consortium to accelerate the photovoltaic module reliability learning cycle *PRX Energy* 3 (2024) 1.

[4] M. Theristis, K. Anderson, J. Ascencio-Vasquez, J.S. Stein, How climate and data quality impact photovoltaic performance loss rate estimations, Sol. RRL 8 (2024).

[5] A. Louwen, S. Lindig, G. Chowdhury, D. Moser, Climate- and technology-dependent performance loss rates in a large commercial photovoltaic monitoring dataset, Sol. RRL 8 (2024).

[6] L. Karttunen, S. Jouttijärvi, A. Poskela, H. Palonen, H. Huerta, M. Todorović, S. Ranta, K. Miettunen, Comparing methods for the long-term performance assessment of bifacial photovoltaic modules in Nordic conditions, Renew. Energy 219 (2023) 119473.

[7] A. Ameur, A. Berrada, A. Bouaichi, K. Loudiyi, Long-term performance and degradation analysis of different PV modules under temperate climate, Renew. Energy 188 (2022) 37–51.

[8] S. Gulkowski, J.V. Muñoz Díez, J. Aguilera Tejero, P. Dragan, G. Nofuentes, A Study on long-term Operation and Performance Loss Rates of Various PV Technologies in Eastern Poland *Renew*, 256, Energy, 2025.

[9] E. Adıgüzel, 10 year performance and degradation analysis of different photovoltaic panels in the Istanbul Türkiye environment, Renew. Energy 251 (2025) 1–12.

[10] D. Atsu, I. Seres, M. Aghaei, I. Farkas, Analysis of long-term performance and reliability of PV modules under tropical climatic conditions in sub-saharan, Renew. Energy 162 (2020) 285–295.

[11] H. Quest, C. Ballif, A. Virtuani, Intrinsic Performance Loss Rate: Decoupling Reversible and Irreversible Losses for an Improved Assessment of Photovoltaic System Performance *Prog. Photovoltaics Res. Appl*, 2024.

[12] R.H. French, L.S. Bruckman, D. Moser, S. Lindig, M van Iseghem, B. Müller, J. S. Stein, M. Richter, M. Herz, W Van Sark, F. Baumgartner, J. Ascencio-Vásquez, D. Bertani, G. Maugeri, A.J. Curran, K. Rath, J. Liu, A. Khalilnejad, M. Meftah, D. Jordan, C. Deline, G. Makrides, G. Georghiou, A. Livera, B. Meyers, G. Plessis, M. Theristis, W. Luo, Assessment of Performance Loss Rate of PV Power Systems, 2021.

[13] S. Lindig, M. Theristis, D. Moser, Best practices for photovoltaic performance loss rate calculations *Prog. Energy* 4 (2022).

[14] D.C. Jordan, C. Deline, S.R. Kurtz, G.M. Kimball, M. Anderson, Robust PV degradation methodology and application, IEEE J. Photovoltaics 8 (2018) 525–531.

[15] S. Lindig, D. Moser, A.J. Curran, K. Rath, A. Khalilnejad, R.H. French, M. Herz, B. Müller, G. Makrides, G. Georghiou, A. Livera, M. Richter, J. Ascencio-Vásquez, M. van Iseghem, M. Meftah, D. Jordan, C. Deline, W. van Sark, J.S. Stein, M. Theristis, B. Meyers, F. Baumgartner, W. Luo, International collaboration framework for the calculation of performance loss rates: data quality, benchmarks, and trends (towards a uniform methodology), Prog. Photovoltaics Res. Appl. 29 (2021) 573–602.

[16] Michael Deceglie, et al., NREL/rdtools: Version 3.0.0-alpha, 5, 2024, 3.0.0-alpha.5.

[17] S. Lindig, A. Louwen, D. Moser, M. Topic, Outdoor PV system monitoring—Input data quality, data imputation and filtering approaches, Energies 13 (2020) 1–18.

[18] H.E. Beck, N.E. Zimmermann, T.R. McVicar, N. Vergopolan, A. Berg, E.F. Wood, Present and future köppen-geiger climate classification maps at 1-km resolution, Sci. Data 5 (2018) 1–12.

[19] C. Monokroussos, Y. Zhang, E.W. Lee, F. Xu, A. Zhou, Y. Zhang, W. Herrmann, Energy performance of commercial c-Si PV modules in accordance with IEC 61853-1, -2 and impact on the annual specific yield, EPJ. Photovoltaics 14 (2023).

[20] M.A. Sevillano-Bendezú, V. Pleshcheva, B. Calsi, L.A. Conde, J. Montes-Romero, J. Aguilera, J. de la Casa, J.A. Töfflinger, Assessing the accuracy of analytical

methods for extracting parameters of different PV module technologies under clear and cloudy sky conditions *Energy Reports* 12 (2024) 4279–4293.
[21] J. Montes-Romero, M. Piliougine, J.V. Muñoz, E.F. Fernández, J. De La Casa, Photovoltaic device performance evaluation using an open-hardware system and standard calibrated laboratory instruments, Energies 10 (2017).
[22] M. Cáceres, A. Firman, J. Montes-Romero, A.R.G. Mayans, L.H. Vera, E. F. Fernández, J. de la Casa Higueras, Low-Cost I–V tracer for PV modules under real operating conditions, Energies 13 (2020) 1–17.
[23] M.A. Zamalloa-Jara, M.Á. Sevillano-Bendezú, C. Ulbrich, G. Nofuentes, R. Grieseler, J.A. Töfflinger, Overirradiance conditions and their impact on the spectral distribution at low- and mid-latitude sites, Sol. Energy 259 (2023) 99–106.
[24] M.A. Sevillano-Bendezú, M. Khenkin, G. Nofuentes, J. de la Casa, C. Ulbrich, J. A. Töfflinger, Predictability and interrelations of spectral indicators for PV performance in multiple latitudes and climates *Sol. Energy* 259 (2023) 174–187.
[25] M.A. Sevillano-Bendezú, L.A. Conde, J. De La Casa, J.A. Töfflinger, Average photon energy assessment based on modelled spectra from the National Solar Radiation Database for Lima, Peru, J. Phys. Conf. Ser. 2180 (2022).
[26] L.A. Conde Mendoza, A. Carhuavilca, R. Perich, J. Montes-Romero, J. Angulo, A. Guerra, E. Muñoz, J. de la Casa, Performance evaluation and characterization of different photovoltaic technologies under the coastal, desertic climate conditions of Lima. Peru *Proceedings of the ISES Solar World Congress 2019*, International Solar Energy Society, Freiburg, Germany, 2019, pp. 1–11.
[27] J.Y. Ye, T. Reindl, A.G. Aberle, T.M. Walsh, Effect of solar spectrum on the performance of various thin-film PV module technologies in tropical Singapore, IEEE J. Photovoltaics 4 (2014) 1268–1274.
[28] J. Chantana, H. Mano, Y. Horio, Y. Hishikawa, T. Minemoto, Spectral mismatch correction factor indicated by average photon energy for precise outdoor performance measurements of different-type photovoltaic modules, Renew. Energy 114 (2017) 567–573.
[29] J. Bryan, T. Silverman, M. Deceglie, M. Mahaffey, P. Firth, Z. Holman, Systematic operating temperature differences between Al-BSF, PERC, and PERT-With-Optimized-Rear-Reflector solar mini-modules due to rear reflectance, IEEE J. Photovoltaics 12 (2022) 293–300.
[30] IEC (International Electrotechnical Commission) 2021 *IEC 61724-1*, Photovoltaic System Performance – Part 1: Monitoring, 2021. Geneva, Switzerland.
[31] IEC (International Electrotechnical Commission), IEC 60904–7:2019, Photovoltaic Devices - Part 7: Computation of the Spectral Mismatch Correction for Measurements of Photovoltaic Devices, 2021. Geneva, Switzerland).
[32] P.M. Rodrigo, E.F. Fernández, F.M. Almonacid, P.J. Pérez-Higueras, Quantification of the spectral coupling of atmosphere and photovoltaic system performance: indexes, methods and impact on energy harvesting, Sol. Energy Mater. Sol. Cells 163 (2017) 73–90.
[33] M. Schweiger, W. Herrmann, A. Gerber, U. Rau, Understanding the energy yield of photovoltaic modules in different climates by linear performance loss analysis of the module performance ratio, IET Renew. Power Gener. 11 (2017) 558–565.
[34] J.R. Angulo, B.X. Calsi, L.A. Conde, J.A. Guerra, E. Muñoz, J. de la Casa, J. A. Töfflinger, Estimation of the effective nominal power of a photovoltaic generator under non-ideal operating conditions, Sol. Energy 231 (2022) 784–792.
[35] K.S. Anderson, C.W. Hansen, W.F. Holmgren, A.R. Jensen, M.A. Mikofski, A. Driesse, Pvlib python: 2023 Project update, J. Open Source Softw. 8 (2023) 5994.
[36] B. James Mokri, J. Cunningham, Practices, Methods and Guidelines to Assess Performance of Existing Systems PV System Performance Assessment, 2014.
[37] S. Lindig, M. Herz, J. Ascencio-Vásquez, M. Theristis, B. Herteleer, J. Deckx, K. Anderson, Review of technical photovoltaic key performance indicators and the importance of data quality routines, Sol. RRL 2400634 (2024) 1–13.
[38] International Energy Agency, Report IEA-PVPS T13-20:2020 Climatic Rating of Photovoltaic Task 13 Performance, Operation and Reliability of Photovoltaic Systems, 2020.
[39] L.A. Conde, J.R. Angulo, M.Á. Sevillano-Bendezú, G. Nofuentes, J.A. Töfflinger, J. de la Casa, Spectral effects on the energy yield of various photovoltaic technologies in Lima (Peru), Energy 223 (2021) 120034.
[40] M. Piliougine, L.E. Garcia-Marrero, K. Lappalainen, G. Spagnuolo, Influence of the temperature on the intrinsic parameters of thin-film photovoltaic modules, Renew. Energy 240 (2025) 122068.
[41] D.C. Jordan, S.R. Kurtz, Photovoltaic degradation Rates—An analytical review, prog. Photovoltaics res. Appl. 21 (2013) 12–29.
[42] S.M. Sze, K.K. Ng, Physics of Semiconductor Devices, John Wiley & Sons, Inc., Hoboken, NJ, USA, 2007.
[43] M. Köntges, S. Kurtz, C.E. Packard, U. Jahn, K. Berger, K. Kato, T. Friesen, H. Liu, M. Van Iseghem, Performance and Reliability of Photovoltaic Systems Subtask 3.2: Review of Failures of Photovoltaic Modules: IEA PVPS Task 13: External Final Report IEA-PVPS, 2014.
[44] A. Sinha, J. Qian, S.L. Moffitt, K. Hurst, K. Terwilliger, D.C. Miller, L.T. Schelhas, P. Hacke, UV-induced degradation of high-efficiency silicon PV modules with different cell architectures, Prog. Photovoltaics Res. Appl. 31 (2023) 36–51.
[45] U. Rau, H.W. Schock, Electronic properties of Cu(In,Ga)Se2 heterojunction solar cells-recent achievements, current understanding, and future challenges, Appl. Phys. A Mater. Sci. Process. 69 (1999) 131–147.
[46] M. Piliougine, P. Sánchez-Friera, G. Petrone, F.J. Sánchez-Pacheco, G. Spagnuolo, M. Sidrach-de-Cardona, New model to study the outdoor degradation of thin–film photovoltaic modules, Renew. Energy 193 (2022) 857–869.
[47] D. Caputo, Degradation and annealing of amorphous silicon solar cells by current injection experiment and modeling, Sol. Energy Mater. Sol. Cells 59 (1999) 289–298.
[48] S. Pradhan, S. Kundu, A. Bhattacharjee, S. Mondal, P. Chakrabarti, S. Maity, Thermal and optical analysis of industrial photovoltaic modules under partial shading in diverse environmental conditions, Sol. Energy 284 (2024) 113097.
[49] D.C. Jordan, S.R. Kurtz, K. VanSant, J. Newmiller, Compendium of photovoltaic degradation rates, Prog. Photovoltaics Res. Appl. 24 (2016) 978–989.